



OPEN ACCESS

EDITED BY

Ayman Al Haj Zen,
Hamad bin Khalifa University, Qatar

REVIEWED BY

William F. Jackson,
Michigan State University,
United States
Erik Josef Behringer,
Loma Linda University, United States
Oana Sorop,
Erasmus Medical Center, Netherlands

*CORRESPONDENCE

Kim A. Dora
kim.dora@pharm.ox.ac.uk

SPECIALTY SECTION

This article was submitted to
Atherosclerosis and Vascular Medicine,
a section of the journal
Frontiers in Cardiovascular Medicine

RECEIVED 28 June 2022

ACCEPTED 26 July 2022

PUBLISHED 12 August 2022

CITATION

Dora KA, Lin J, Borysova L, Beleznai T,
Taggart M, Ascione R and Garland C
(2022) Signaling and structures
underpinning conducted vasodilation
in human and porcine intramyocardial
coronary arteries.
Front. Cardiovasc. Med. 9:980628.
doi: 10.3389/fcvm.2022.980628

COPYRIGHT

© 2022 Dora, Lin, Borysova, Beleznai,
Taggart, Ascione and Garland. This is
an open-access article distributed
under the terms of the [Creative
Commons Attribution License \(CC BY\)](#).
The use, distribution or reproduction
in other forums is permitted, provided
the original author(s) and the copyright
owner(s) are credited and that the
original publication in this journal is
cited, in accordance with accepted
academic practice. No use, distribution
or reproduction is permitted which
does not comply with these terms.

Signaling and structures underpinning conducted vasodilation in human and porcine intramyocardial coronary arteries

Kim A. Dora^{1*}, JinHeng Lin¹, Lyudmyla Borysova¹,
Timea Beleznai¹, Michael Taggart², Raimondo Ascione³ and
Christopher Garland¹

¹The Vascular Pharmacology Group, Department of Pharmacology, University of Oxford, Oxford, United Kingdom, ²Biosciences Institute, Newcastle University, Newcastle upon Tyne, United Kingdom, ³Bristol Heart Institute and Translational Biomedical Research Centre, University of Bristol, Bristol, United Kingdom

Background: Adequate blood flow into coronary micro-arteries is essential for myocardial function. Here we assess the mechanisms responsible for amplifying blood flow into myogenically-contracting human and porcine intramyocardial micro-arteries *ex vivo* using endothelium-dependent and -independent vasodilators.

Methods: Human and porcine atrial and ventricular small intramyocardial coronary arteries (IMCAs) were studied with pressure myography and imaged using confocal microscopy and serial section/3-D reconstruction EM.

Results: 3D rendered ultrastructure images of human right atrial (RA-) IMCAs revealed extensive homo- and hetero-cellular contacts, including to longitudinally-arranged smooth muscle cells (l-SMCs) found between the endothelial cells (ECs) and radially-arranged medial SMCs (r-SMCs). Local and conducted vasodilatation followed focal application of bradykinin in both human and porcine RA-IMCAs, and relied on hyperpolarization of SMCs, but not nitric oxide. Bradykinin initiated asynchronous oscillations in endothelial cell Ca^{2+} in pressurized RA-IMCAs and, as previously shown in human RA-IMCAs, hyperpolarized porcine arteries. Immunolabelling showed small- and intermediate-conductance Ca^{2+} -activated K^+ channels (K_{Ca}) present in the endothelium of both species, and concentration-dependent vasodilation to bradykinin followed activation of these K_{Ca} channels. Extensive electrical coupling was demonstrated between r-SMCs and l-SMCs, providing an additional pathway to facilitate the well-established myoendothelial coupling. Conducted dilation was still evident in a human RA-IMCA with poor myogenic tone, and heterocellular contacts were visible in the 3D reconstructed artery. Hyperpolarization and conducted vasodilation was also observed to adenosine which, in contrast to bradykinin, was sensitive to combined block of ATP-sensitive (K_{ATP}) and inwardly rectifying (K_{IR}) K^+ channels.

Conclusions: These data extend our understanding of the mechanisms that coordinate human coronary microvascular blood flow and the mechanistic overlap with porcine IMCAs. The unusual presence of l-SMCs provides an additional pathway for rapid intercellular signaling between cells of the coronary artery wall. Local and conducted vasodilation follow hyperpolarization of the ECs or SMCs, and contact-coupling between l-SMCs and r-SMCs likely facilitates this vasodilation.

KEYWORDS

human coronary arterioles, coronary microvascular function, myogenic tone, Ca²⁺ signaling, conducted vasodilation, endothelial cell, bradykinin, adenosine

Introduction

Cardiac function is critically dependent on the effective autoregulation of blood flow through the myocardium, and is controlled by the small arteries and arterioles of the microcirculation (1, 2). However, routine assessment of the functional state of the microcirculation is difficult *in vivo*, highlighting the importance of unraveling intramyocardial coronary artery (IMCA) signaling mechanisms under defined conditions *ex-vivo* (3–6).

Blood flow autoregulation relies largely on metabolic modulation of the inherent spontaneous myogenic activity, or tone, of small arteries. To become effective, local vasodilation must spread over distance. This is achieved by the phenomenon of conducted vasodilation, first recognized in skeletal muscle (7, 8). Conducted vasodilation usually relies on the spread of hyperpolarizing current along the endothelium, away from the local site of initiation, then back to the adjacent smooth muscle via heterocellular, myoendothelial gap junctions. Hyperpolarization of the smooth muscle reduces the open probability of voltage-gated calcium channels (VGCCs) affecting vasodilation (9). It follows that to be effective, locally released vasodilator autacoids (for example in ischaemic regions) must stimulate smooth muscle hyperpolarization, either directly or indirectly *via* the endothelium.

The ability to sustain conducted vasodilation is poorly characterized in coronary arteries, to date shown in porcine sub-epicardial coronary arterioles and human intra-pectinate coronary arterioles (10, 11). In the latter, bradykinin initiated conducted vasodilation by activating endothelium-dependent hyperpolarization (EDH), with endothelial nitric oxide (NO) suggested to facilitate this conduction to facilitate this conduction (10). Bradykinin is an endogenous vasodilator in the coronary circulation and during vasoconstrictor-induced tone in human coronary arterioles stimulates hyperpolarization by activating endothelial calcium-activated potassium channels (K_{Ca}) (12, 13).

The present study was designed to extend the very limited data available regarding conducted vasodilation in

myogenically contracting human and pig coronary IMCAs, probing whether similar underlying mechanisms operate. We also aimed to establish whether the intra-pectinate arteries routinely available from discarded human atrial appendage, and less available ventricular micro-arteries from organ donors, behave in a similar manner to equivalent porcine arteries. Our data link to previous studies with porcine ventricular sub-epicardial and sub-endocardial arterioles and large epicardial coronary arteries (11, 14–16) and indicate that porcine arteries provide an appropriate non-primate alternative to human arteries for cardiovascular studies (17).

Methods

Human and porcine study design and isolation of IMCAs

Human right atrial appendage biopsies

We used arteries from 45 patients (aged ≥ 25 and ≤ 80 years), 43 with valvular disease requiring either aortic valve replacement (AVR) or mitral valve repair/replacement (MVR) or both (AVR+MVR) and 3 with obstructive coronary disease, each undergoing elective or urgent cardiac surgery, a subset of patients from a previous study (18). These patients were chosen for this study based on their arteries developing $>10\%$ myogenic tone which was fully reversed with bradykinin, our previously defined inclusion criteria for viable arteries (18). Patient demographics and exclusion criteria are outlined in Table 1. We included data from two additional patients whose arteries had contractile dysfunction, for comparison purpose only, with the same exclusion criteria. The patient details are provided in Table 2. The University Hospital Bristol NHS Foundation Trust sponsored the study in Bristol, and the trial was approved by the Oxford Research Ethics Committee and extended to the Bristol site. The research complies with the Helsinki Declaration. RA biopsy samples from recruited patients were

TABLE 1 Patient demographics and exclusion criteria ($n = 45$)*.

			<i>n</i>	%
Sex	Female/male	17/28	45	
Age, yrs	mean \pm SD	62 \pm 12	45	
Surgical procedure	Valve repair/replacement		43	96
	CABG		3	7
Underlying risk factors	Hypertension		21	47
	Hypercholesterolemia		18	40
	Previous MI		4	9
	Decompensated CHF		1	2
	Large coronary artery disease		3	7
	Diabetes Mellitus		8	18
	Smoking History (<1 month)		4	9
	None of the above		18	40
Baseline medications	Statins		21	47
	Diuretics		11	24
	Anticoagulation		7	16
	Beta-blockers		14	31
	ACE-inhibitors		13	29
	Aspirin		12	27
Exclusion criteria	Age <25 years or >80 years			
	Pulmonary hypertension >50 mmHg			
	Impaired right ventricular function			
	Severely dilated atria (>5.0 cm)			
	Need for redo cardiac surgery			
	Need for ascending/root aortic surgery			
	Emergency surgery			
	Acute endocarditis			
	Infection, known HIV, Hepatitis A, B, C			
	Cancer or receiving chemotherapy			
	Immune disease			
	Ongoing pregnancy			

SD, standard deviation; CHF, Congestive Heart Failure; AVR, aortic valve replacement; MVR, mitral valve repair/replacement; CABG, coronary artery bypass grafting; HIV, human immunodeficiency virus. These data form a subset of 88 patients recruited for a full assessment of vascular reactivity (18).

*Two additional patients with the same exclusion criteria were included in this study for comparison purposes only, experimental data were not included in data summaries (patient demographics are provided in Table 2).

transported to Oxford under a material transfer agreement under strict packaging, temperature regulation ($\sim 10^{\circ}\text{C}$) and time-limit conditions.

Human left ventricle biopsies from organ donors

Human heart tissue (Newcastle) was provided by The Newcastle Institute of Transplantation Tissue Biobank, the same patients as in our previous study (18). Once the biopsy was removed, the protocols matched the strict procedures used for the human cardiac surgery RA biopsies.

Porcine right atrial appendage and left ventricle biopsies

All the animal procedures were undertaken at the University of Bristol large animal facilities. All procedures were approved by University of Bristol Research Ethics Committee and performed in accordance with the Guide for the Care and Use of Laboratory Animals (19), the United Kingdom Animal (Scientific Procedures) Act, 1986, and conform to the guidelines from Directive of the European Parliament on the protection of animals used for scientific purposes. The animals recruited are the same as from our previous study (18). All animals were undergoing cardiac surgery with right atrial biopsies collected prior to cardiopulmonary bypass, and left ventricular biopsies

TABLE 2 Human RA-IMCAs processed for SBF-SEM arteries ($n = 3$).

Artery	Patient demographics	MT (%)	Vasodilation to 10 nM BK (%)	Conducted dilation to BK (Y/N)
#1	Female, 69 yrs, NT, NL, valve surgery; LV function good, >50% Meds: Statins	14.7	42.0	Y
#2*	Male, 52 yrs, HT, HL, CABG surgery; LV function poor, <30% Meds: Beta-blocker, ACE-inhibitor, diuretic, anticoagulant, statin	5.8	0.0	Y
#3*	Female, 81 yrs, HT, HL, valve surgery; LV function good, >50% Meds: ACE-inhibitor, diuretic, statin	0.0	0.0	-

In addition to one viable artery (Artery #1), arteries from two additional patients were isolated, cannulated and pressurized for assessment of vascular reactivity and then processed for SBF-SEM. Arteries #2 and #3 were not viable (MT <10%) and therefore data were not included in data summaries; they are shown for comparison purposes only. Data are presented in the Figures and Movies listed. MT, myogenic tone; BK, bradykinin; NT, normotensive; HT, requiring treatment for hypertension; NL, normal lipids; HL, requiring treatment for hypercholesterolaemia; Meds, baseline medications.

from the endocardial surface collected at termination. All porcine biopsies were collected, packed and promptly couriered to Oxford using the same approach used for human RA and LV biopsies.

While arteries from each biopsy were all used in our previous study (18), each artery was subsequently used for additional protocols to form the new data presented here. The previously published values for myogenic tone and control dilation responses to bradykinin were necessarily included in this study.

Once in the laboratory, arteries were carefully cleared of surrounding tissue, avoiding side branches, and transferred to a myograph chamber (2 mL, RC-27 Warner Instruments, Hamden, CT) containing chilled MOPS buffer, held within the stage of an Olympus microscope, as previously described (18).

Vascular reactivity of *ex vivo* pressurized IMCAs

Diameter studies

In all studies, IMCAs were mounted onto pipettes at each end with one end open to 80 mmHg (generated by gravity) and the other end closed to flow, meaning that luminal flow was effectively prevented [limited to leak across the ECs (18) and small changes during changes in diameter]. IMCAs were visualized using Olympus linescan confocal microscopes (FV300, FV500, FV1000 or FV1200). When studying function, arteries were imaged with transmitted light using a 10x Olympus objective and recorded using Fluoview software (Olympus, Tokyo, Japan) at 1 Hz, as previously described (18, 20). Myogenic tone was assessed as the tone developed in response to 80 mmHg luminal pressure, relative to the maximum diameter

of arteries as previously described (18). Of the original study ($n = 88$ patients) which included many arteries with poor myogenic tone ($n = 39$), only arteries with >10% myogenic tone were used for this study ($n = 45$ of possible $n = 49$ patients). Endothelial cell (EC) function was assessed using bradykinin; arteries with >95% dilation to 1 nM and 1 μ M bradykinin in porcine and human RA-IMCAs, respectively, were used. Values are the mean \pm SEM of n patient or pig samples, one artery per sample unless otherwise stated.

Cumulative concentration response curves (CRCs) to bradykinin were obtained by addition of <20 μ L doses of concentrated bradykinin (in MOPS buffer) to the edge of the warmed, static bath in a 2 mL imaging chamber, with gentle trituration to mix to the desired bath concentration, in 10-fold steps. The artery was exposed to each concentration for up to 120 s, which allowed peak responses to be recorded. Blockers were added to the superfusion flow for at least 20 min prior to commencing CRCs for dilator agonists, the vehicle not having any effect against MT or agonist responses.

Conducted dilation experiments were performed in arteries with one end closed to luminal flow to reduce the possible influence of shear stress. To limit agonist delivery to a confined region of the artery (termed downstream end), the superfusion flow rate longitudinally along the outside of arteries was near 2 mL/min. Bradykinin (10 μ M or 1 μ M for human or porcine IMCAs, respectively) or adenosine (100 μ M) was delivered as a short bolus using a pressure or syringe pump positioned at the downstream end of the artery and near the imaging midplane of the artery (21). Note that this method of applying an agonist is akin to a bolus dose rather than steady state concentration. The bradykinin is diluted before reaching the lumen of the artery, and is delivered transiently, so the concentrations required to evoke dilation are higher than those when added to a

static bath. Our previous studies have demonstrated that the direction of the superfusion flow does not always represent the direction of flow across the artery, due to the turbulence generated by the cannulating pipettes (21). Therefore, to ensure the delivery of agonists remained at the downstream end of the arteries, carboxyfluorescein (250 nM) was included in the pump micropipette to report the direction of agonist flow using confocal microscopy. The pump micropipette was moved to the other end of the artery as flow direction necessitated (21). This meant that we were able to visualize the delivery of agonists and subsequent conducted vasodilation across the entire artery assessing vasodilation at all points along the artery segment following a single, local application of the agonist. When using a 10x objective, >1,200 μm lengths of arteries were imaged in a field of view for simultaneous diameter and fluorescence measurements at positions 0–1,000 μm from the stimulating pipette. The default imaging field was *circa* 1,440 x 440 μm , at 1.4 $\mu\text{m}/\text{pixel}$. The delivery of agonist ceased as the artery dilated, which was within a few seconds. The same pipette position and delivery protocol was used for each given artery, with and without the addition of blockers to the superfusion solution. To compare the decay of dilation along each artery, data were normalized to the response at 200 μm from the delivery pipette, a site considered upstream to direct agonist delivery and more dependent on the spread of hyperpolarizing current. Thus the simultaneous values for diameter along the artery were obtained when the vasodilation to the agonist was 80% of maximal diameter at 200 μm , in a manner similar to previously (22, 23).

EC intracellular Ca^{2+} studies

After establishing the artery vasoreactivity, changes in arterial EC intracellular Ca^{2+} were imaged using the fluorescent Ca^{2+} -indicators Oregon Green 488 BAPTA-1 or fluo-8 as previously (18). After excitation at 488 nm, fluorescence emission intensity was captured from at least 10 cells in the field of view at the bottom surface of arteries at an acquisition rate of 3 Hz using Fluoview software (version 3.5). Following a baseline of > 30 s, 0.1–100 nM bradykinin was added to generate cumulative CRCs in a static bath. Peak responses were observed within 90 s. Up to 6 cells per field of view were analyzed and averaged to give one *n* value per artery. Data were analyzed offline using MetaMorph software (version 7.7.4.0, Molecular Devices). Subcellular regions of interest (diameter $\sim 5 \mu\text{m}$) were positioned both within active cells and away from cells (latter for background intensity) to obtain fluorescence intensity over time. Background-subtracted raw data are expressed as relative fluorescence (F/F_0) by dividing fluorescence intensity (*F*) by an average baseline fluorescence intensity F_0 . Values are summarized as the mean \pm SEM, with *n* representing the number of arteries studied.

SMC intracellular Ca^{2+} studies

Animal use was approved by the University of Oxford Ethical Committee and complied with the Animals (Scientific Procedures) Act 1986. Animals were housed in a temperature-controlled environment with a 24-h light-dark cycle and water *ad libitum*. These studies comply with ARRIVE guidelines (24, 25). Male Wistar rats (230–280 g) were killed by exposure to rising concentration of CO_2 , and confirmed by cervical dislocation [as specified by Schedule 1 of the Animals (Scientific Procedures) Act 1986, UK]. The heart was pinned and incision into the right ventricle exposed the septal artery, which was dissected and mounted into a confocal wire myograph (model 120CW, Danish Myo Technology A/S) and in Krebs solution containing (in mM): 118 NaCl, 25 NaHCO_3 , 3.6 KCl, 1.2 $\text{MgSO}_4 \cdot 7\text{H}_2\text{O}$, 1.2 KH_2PO_4 , 1.25 CaCl_2 , 11 glucose and gassed with 21% O_2 , 5% CO_2 , with N_2 . The solution temperature was raised to 37°C, and the artery normalized to a resting tension equivalent to that generated at 90% of the diameter of the vessel at 80 mmHg (26). Following an equilibration period of 1 h, endothelial function was assessed by >90% relaxation to 100 nM acetylcholine from pre-constriction with phenylephrine. Viable arteries were loaded with the calcium-sensitive fluorescent dye Calbryte 520 (AAT Bioquest) [2.5 μM ; dissolved in DMSO and 0.03% (w/v) Pluronic F-127] for 30 min at 30°C, then incubated in Krebs buffer for 30 min at 37°C to allow de-esterification. After excitation at 488 nm, the fluorescence emission intensity at 513–563 nm was recorded from the bottom surface of arteries using a spinning disc confocal microscope (Yokogawa CSU22) fitted with an Andor iXON DV887ECS-BV camera mounted on an Olympus IX70 inverted microscope using a water immersion objective (x40, aperture 0.8, working distance 3.3 mm; Olympus) and images (430 x 420 pixels, 35 Hz) were stored for offline analysis (iQ version 3.5, Andor Bioimaging Division, UK; MetaMorph version 7.7.4.0, Molecular Devices). Following background subtraction, average relative changes in $[\text{Ca}^{2+}]$ were calculated as changes in intensity of fluorescence divided by fluorescence at time 0 s (F/F_0), within selected cell regions and the whole field. Data are expressed either as relative fluorescence (F/F_0) or the frequency of Ca^{2+} events observed per min.

Electrophysiology in *ex vivo* tensioned coronary IMCAs

Porcine RA-IMCAs were dissected as for pressure myography, but were instead mounted in a wire myograph, for simultaneous measurement of SMC membrane potential and isometric tension, as previously for rat coronary arteries (26). Arteries ($\sim 2 \text{ mm}$ long) were normalized to a resting tension equivalent to that generated at 90% of the inner diameter of the vessel at 80 mmHg, treated with 45 mM K^+ and washed. SMC membrane potential and tension were recorded through a pre-amplifier (Neurolog system, Digitimer Ltd., U.K.) linked to

a MacLab data acquisition system (AD Instruments Model 4e, New Zealand) and LabChart software (v7.2.5, AD Instruments, New Zealand). Individual SMCs were impaled with sharp glass microelectrodes (backfilled with 2 M KCl; tip resistances *circa* 60 M Ω), observed as a rapid deflection toward the resting membrane potential, near -50 mV. The chamber was maintained at 37°C .

3D structure of *ex vivo* pressurized coronary IMCAs

Electron microscopy

IMCAs processed for electron microscopy were fixed at the end of functional assessment for myogenic tone and vasomotor responses, including conducted dilation, as previously described (18). In this study the previously obtained serial SBF-SEM images acquired were handled and processed for segmentation with Microscopy Image Browser (MIB), Helsinki (27). Individual cells were followed in all three dimensions for reconstructions with MIB. The cells were manually traced in MIB using the “brush” drawing tool and aided by interpolation. The individual cell models were compiled using Imaris (version 9.8.0) for presentation.

Confocal fluorescence microscopy

Studies of K_{Ca} channel expression were carried out following fixation of cannulated IMCAs at 80 mmHg with 2% (w/v) paraformaldehyde for 10 min at $36.6 \pm 0.3^{\circ}\text{C}$, washing with phosphate-buffered saline before further study. Whilst still cannulated, IMCAs were exposed to antibodies in the incubation chamber to label from the outside of arteries, and were also pumped into the lumen of arteries to label the ECs and inner SMC layers, as previously (18, 28). Primary antibodies were as follows: 1:100 rabbit polyclonal anti-rat $\text{K}_{\text{Ca}3.1}$ (aa 350–363; Alomone Laboratories, APC-064); 1:100 mouse monoclonal anti-human $\text{K}_{\text{Ca}3.1}$ (third extracellular loop; Alomone Laboratories, ALM-051); and 1:100 rabbit polyclonal anti-human $\text{K}_{\text{Ca}2.3}$ (aa 2–21, Alomone Laboratories, APC-025). Secondary antibodies were as follows: 1:100 goat anti-rabbit IgG, Invitrogen, A-11008; or 1:100 chicken anti-mouse IgG, Invitrogen, A-21200. Nuclei and elastin (including the internal elastic lamina, IEL) were stained with 15 μM propidium iodide and 200 nM Alexa Fluor 633 hydrazide (Molecular Probes, A-30634), respectively (28). Arteries were excited at 488, 546, and 633 nm; the fluorescence emitted at 505–525, 560–620, and 655–755 nm was acquired through a water immersion objective (1.15 NA, Olympus, $1,024 \times 1,024$ pixels) using a laser scanning confocal microscope (FV1000 or FV1200; Olympus). z-stacks through the artery wall were obtained at 0.20- μm increments

by using Fluoview Software (FV10-ASW 3.0; Olympus) and reconstructed in Imaris Software (version 8.0.2; Bitplane).

Statistical analysis

Statistical analysis was performed using GraphPad Prism software (version8, GraphPad Software, La Jolla, USA), where $P < 0.05$ was considered significant. All specimens collected were analyzed and no experimental data that passed the inclusion criteria ($\geq 10\%$ myogenic tone and dilation to bradykinin) were excluded from the study. Formal statistical comparisons on paired data first tested for Gaussian distributions (D’Agostino and Pearson omnibus normality test), which confirmed non-parametric tests should be used. Values are given as mean \pm SEM unless otherwise specified.

Results

Characteristics of human and porcine RA-IMCAs

The human and porcine RA appendage biopsies used for experiments in this study were a subset of those used previously (18) (Table 1) with 2 additional patients (Table 2, data not included in diameter summaries). The maximum inner diameter of human arteries was $153 \pm 6 \mu\text{m}$ and they developed $23.3 \pm 1.8\%$ myogenic tone to $117 \pm 5 \mu\text{m}$ ($n = 45$). For comparison purposes, a limited number of IMCAs were also obtained from human organ donors (OD-RA-IMCAs). These had a maximum inner diameter of $152 \pm 10 \mu\text{m}$ and each developed $>10\%$ MT ($32.1 \pm 7.2\%$ MT, $n = 3$) (18). Of the 39 porcine biopsies, all arteries developed $>10\%$ MT and fully dilated to bradykinin, matching the criteria for inclusion. The maximum inner diameter of porcine arteries was $203 \pm 11 \mu\text{m}$ developing $25.4 \pm 1.5\%$ MT to reach stable resting diameters of $154 \pm 10 \mu\text{m}$ ($n = 39$).

Characteristics of human and porcine LV-IMCAs

We were able to source a limited number of ventricular biopsies obtained from organ donors, and pigs at the time of sacrifice, for comparison of bradykinin responses between heart chambers and across species. The left ventricular IMCAs from human organ donors (OD-LV-IMCAs) had a maximum inner diameter of $272 \pm 56 \mu\text{m}$ and each developed $>10\%$

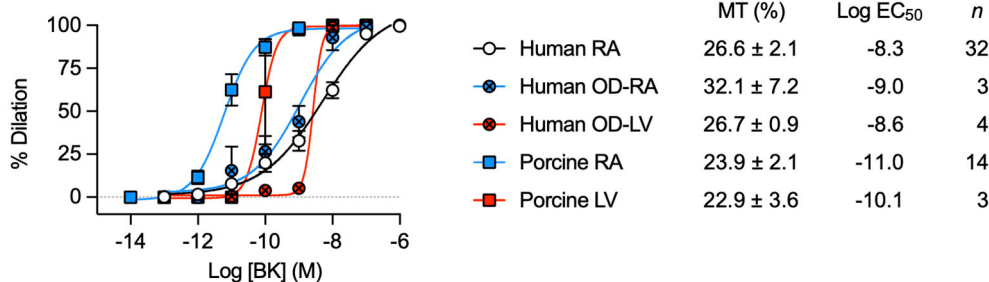


FIGURE 1

Characterization of dilation to bradykinin in IMCAs mounted in a pressure myograph. Comparison of control concentration-dependent BK vasodilation responses across species and heart chambers. Data from human and porcine RA-IMCAs are compared to organ donor (OD) RA and left ventricle (LV) arteries, and porcine LV arteries. Values specific to the experiments performed in this study for both MT and the non-organ donor RA-IMCA concentration response curves to BK are modified from Dora et al. (18).

MT ($26.7 \pm 0.9\%$ MT, $n = 4$) (18). The porcine LV-IMCAs had a maximum inner diameter of $248 \pm 38 \mu\text{m}$ and each developed $>10\%$ MT ($22.9 \pm 3.6\%$ MT, $n = 3$) (18).

Comparison of EC-dependent dilation in human and porcine RA/LV-IMCAs

The percentage concentration-dependent vasodilation of developed MT to bradykinin was remarkably similar between RA samples from patients undergoing elective cardiac surgery and from the organ donors (Figure 1). The mean age of each group was similar (elective surgery 62 ± 12 years, $n = 45$; organ donors 63 ± 8 years, $n = 3$; mean \pm SD). These data support the use of patients undergoing this type of surgery (Table 1), as individuals without significant coronary microvascular disease. The magnitude of developed MT in porcine RA-IMCAs was similar, yet the concentration-dependent vasodilation to bradykinin in human arteries was *circa* 50-fold (LV) to 500-fold (RA) right-shifted compared to the porcine arteries (Figure 1). The similarity in MT and EC-dependent characteristics of organ donor LV-IMCAs, organ donor RA-IMCAs and elective surgery patient RA-IMCAs gave security to proceed with the more readily available elective surgery patients for the remainder of this study.

Structural observations in coronary IMCAs

Some of the arteries used to assess conducted vasodilation to bradykinin were subsequently fixed and examined

microscopically at high resolution. Cell-cell contacts were clearly visible between smooth muscle cells, endothelial cells and between the two cell types (Figure 2). These sites of contact are the potential location of gap junctions, which are essential for local and conducted homo- and heterocellular electrical coupling and hence underpin conducted vasodilation.

Conducted vasodilation initiated by focal application of bradykinin

The focal delivery of bradykinin (indicated by co-release of fluorescent carboxyfluorescein) to one end of either human or porcine RA-IMCAs evoked vasodilation that spread along the arteries with minimal decline for at least $1,000 \mu\text{m}$ from the site of application (Figure 3). The age of patients did not influence the decay with distance along the artery ($n = 9$, Figure 4A). The local and conducted vasodilation to bradykinin was not affected by the presence of $100 \mu\text{M}$ L-NAME to block endothelial NO synthase or $30 \mu\text{M}$ Ba^{2+} , a concentration that selectively blocks vascular inwardly rectifying K channels (K_{IR}). In contrast, vasodilation to bradykinin was abolished by raised extracellular K^+ (45 mM). These experiments are summarized in Figures 3H,I. Experiments were also performed in the presence of TRAM-34 and apamin to block endothelial K_{Ca} channels. As shown previously in human RA-IMCAs (10), both local and conducted vasodilation were markedly reduced (Figure 4E). We did not pursue this aspect further, but it was clear there was some variability as in combination TRAM-34 (to block IK_{Ca} , $\text{K}_{\text{Ca}3.1}$) and apamin (to block SK_{Ca} , $\text{K}_{\text{Ca}2.3}$) either blocked local and conducted responses (3 of 5 arteries) or had little influence (Figure 4F).

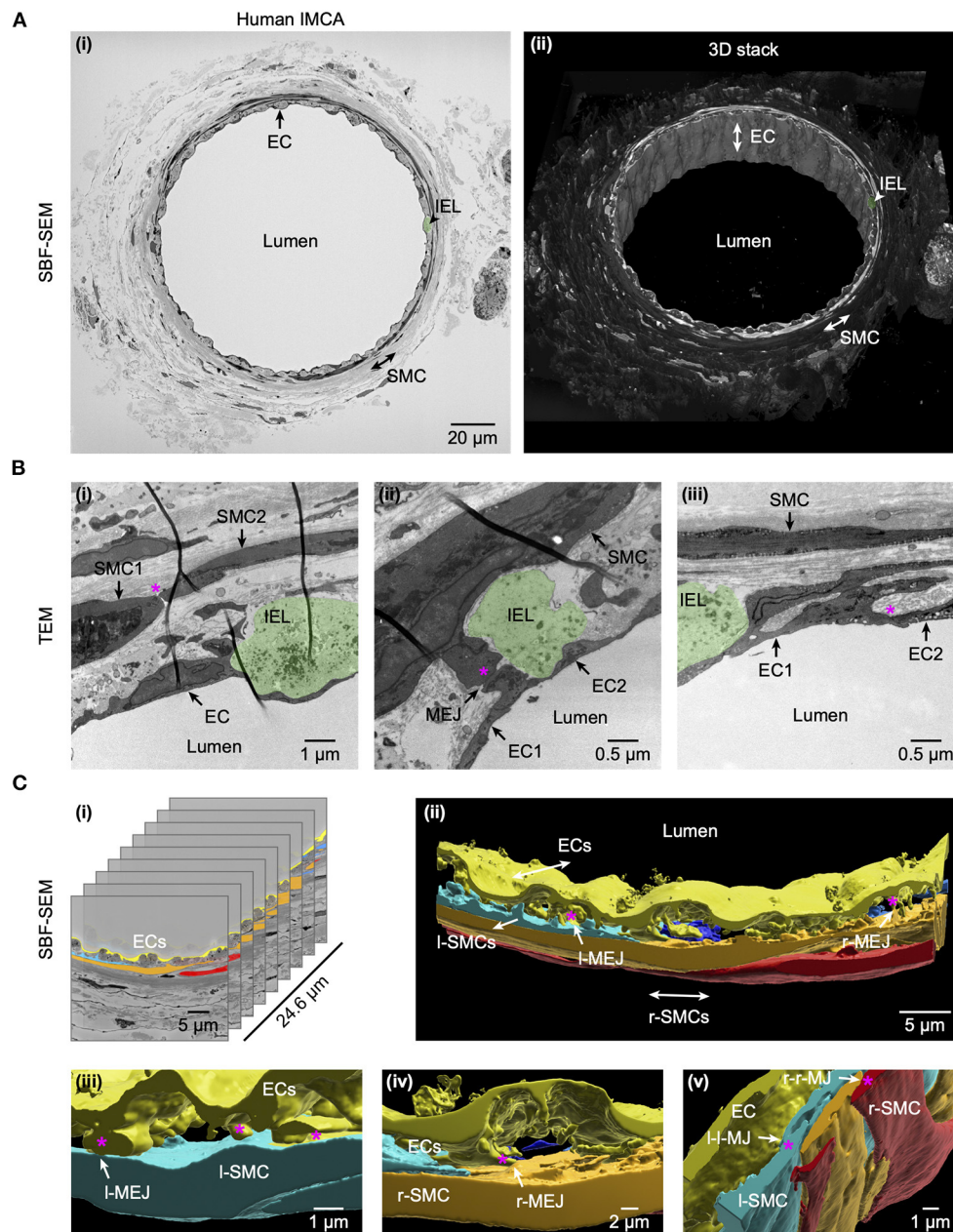


FIGURE 2

Cell-cell contact sites in a human RA-IMCA with good contractile function. The artery (Artery #1, Table 2) was first used for functional experiments (included in Figures 3, 7) and then while still cannulated and pressurized, processed for both serial block face scanning electron microscopy (SBF-SEM, A) and transmission electron microscopy (TEM, B). At low resolution (A) it is clear that 1–2 layers of SMCs surround the ECs and internal elastic lamina (IEL). Arrows indicate the same EC, and position of SMCs and IEL in both the 2D- (left) and 3D- (right) images. The IEL comprises longitudinal strings of elastin (examples in Figures 5A, 6A,B), one example is highlighted in green in all panels. A movie through the 3D z-stack at low and higher resolution is available at Dora et al. (18). Higher resolution images (B) were obtained before processing for SEM, and showed clear contact sites between SMCs, between SMC and ECs, and between ECs, an example indicated by the asterisk in each panel. Representative of 5 arteries which developed myogenic tone and responded to BK (18). (C) The cell-cell contact sites were also visible in the SBF-SEM images (Supplementary Video 1). Individual cells were 3D rendered and are shown superimposed on the original images (i) and as the reconstructed artery walls (ii–v). Longitudinally arranged SMCs (l-SMCs) are shown in blue (see Figure 12), and circumferential radial SMCs (r-SMCs) in orange and red; each of which contacted each other and endothelial cells. Examples are indicated by r-MEJ, r-SMC to EC junction; I-MEJ, I-SMC to EC junction; I-I-MJ, I-SMC to I-SMC junction; r-r-MJ, r-SMC to r-SMC junction.

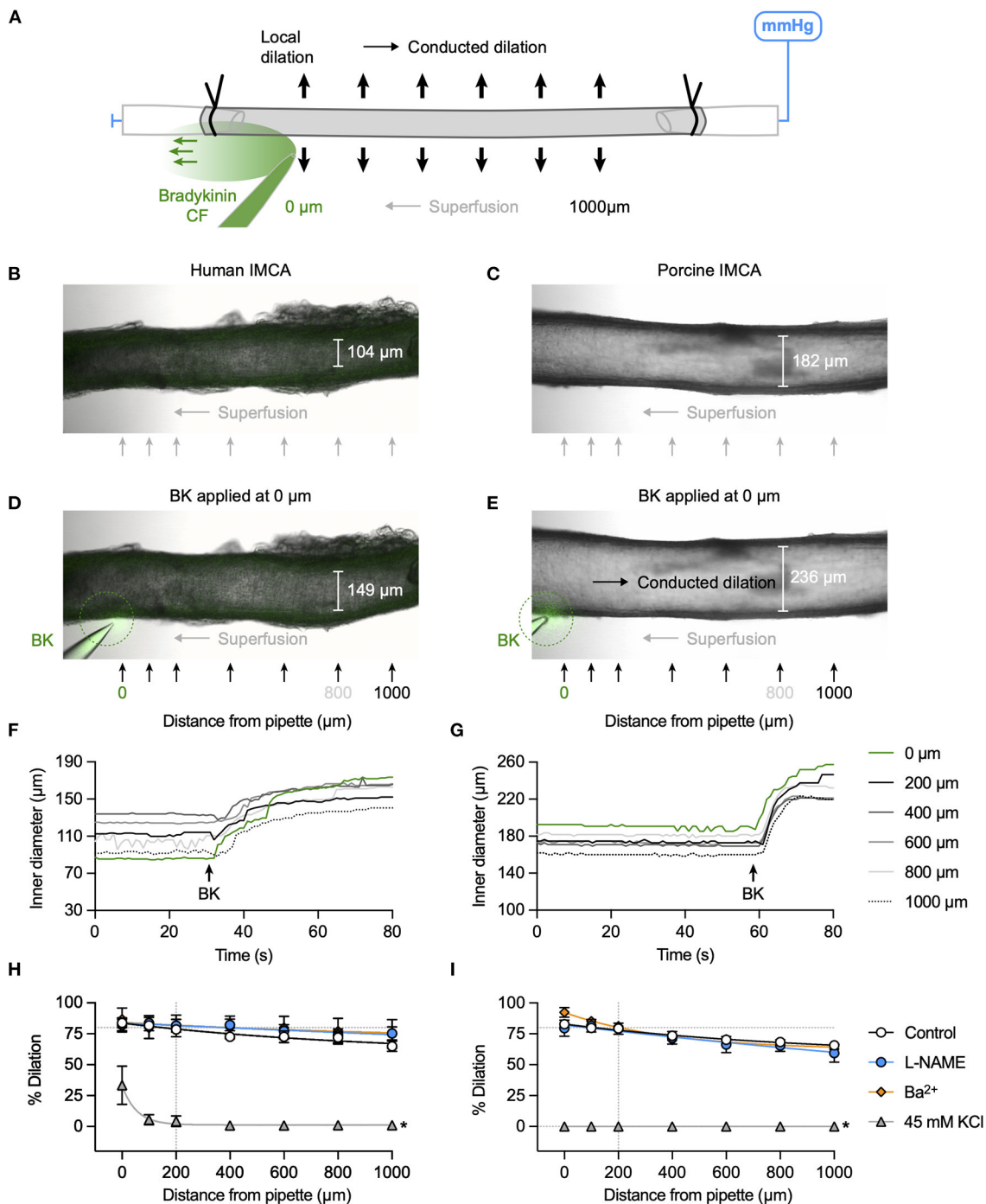
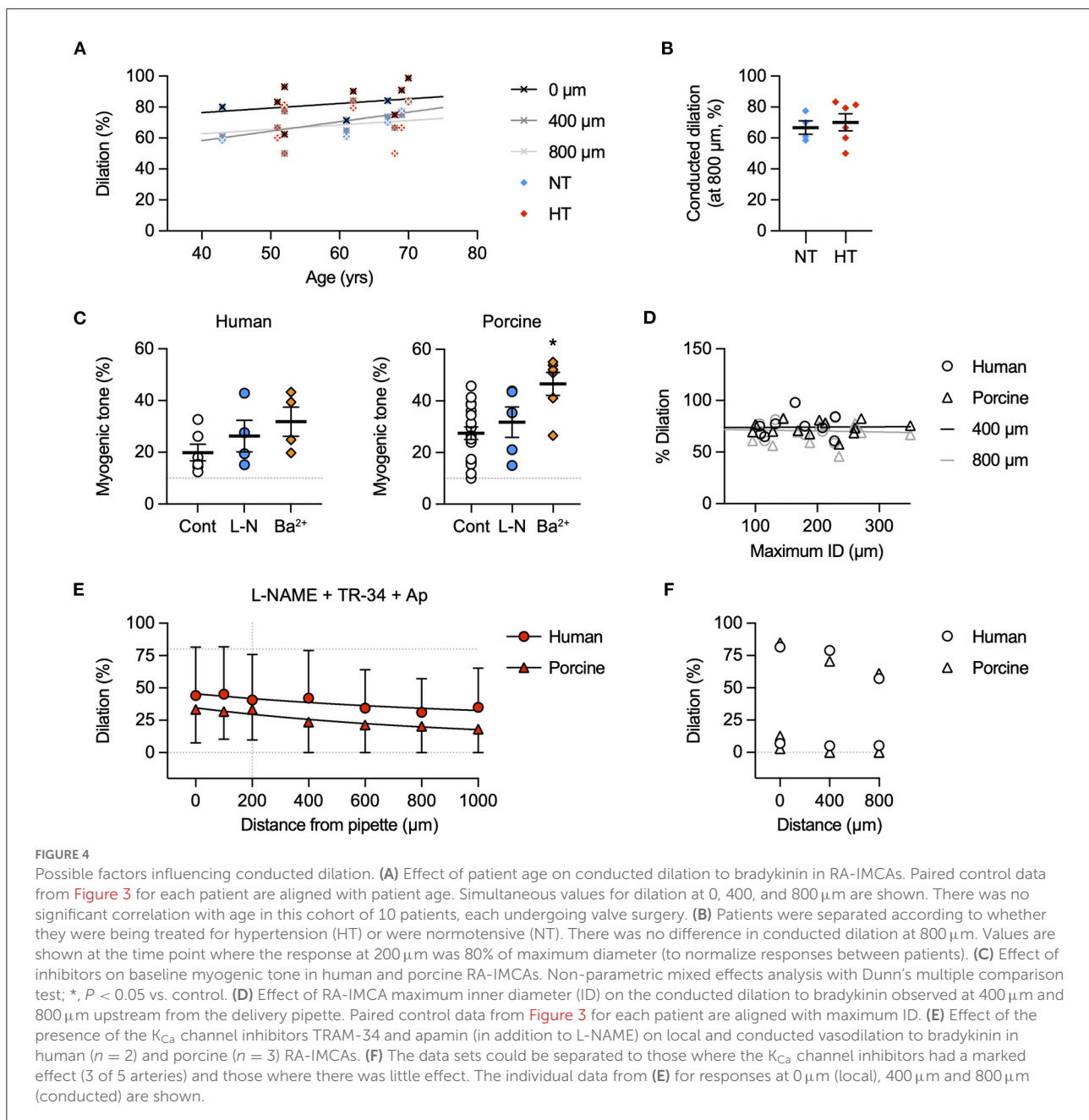


FIGURE 3

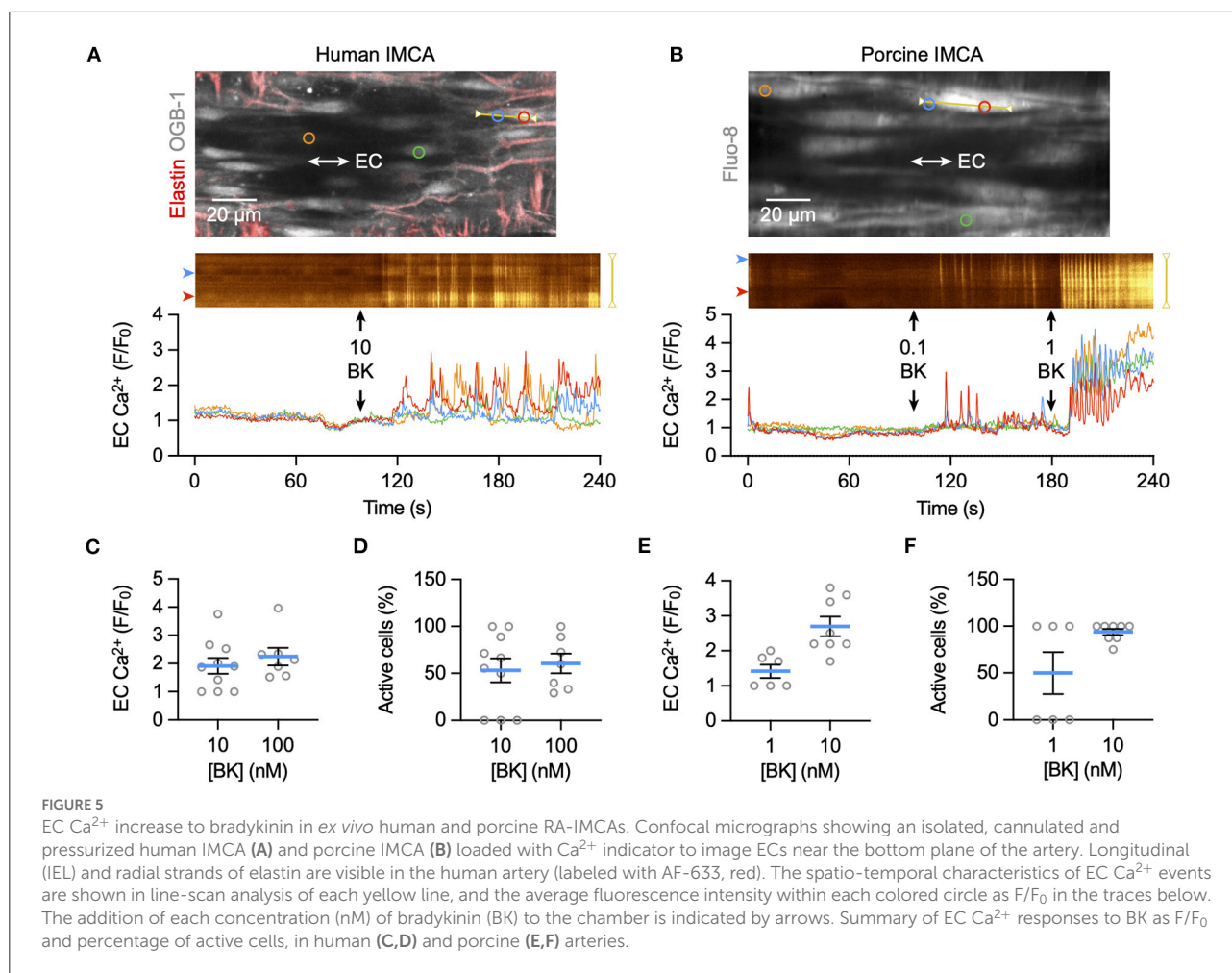
K^+ channel-mediated vasodilation underlies conducted dilation of human and porcine RA-IMCAs. (A) Schematic of experimental setup with direction of flow of bradykinin (BK) indicated by carboxyfluorescein (CF). Micrographs showing an isolated, cannulated and pressurized human (B) and porcine (C) artery. Focal application of BK (and CF, green) to the downstream end of the artery against the direction of superfusion flow caused local and conducted dilation in both human (D) and porcine (E) arteries. The corresponding time course of responses are shown in (F,G), and [Supplementary Videos S2, S3](#). A bolus of bradykinin was delivered at the point indicated by the arrow, and simultaneous inner diameter measured locally (0 μm) and up to 1,000 μm upstream, positions indicated by arrows in (D,E). The same human artery used for $K_{Ca}3.1$ immunolabel in [Figure 6A](#). Summary graphs show that compared to control ($n = 9, 14$) neither L-NAME (100 μM, $n = 3, 6$) nor Ba^{2+} (30 μM, $n = 3, 3$) affected local or conducted dilation, whereas depolarization to 45 mM KCl abolished conducted dilation ($n = 3, 6$) in human (H) and porcine (I) arteries, respectively. Non-parametric mixed effects analysis with Sidak's multiple comparison test; * $P < 0.05$ vs. control.



Bradykinin activates EC Ca^{2+} elevation, K_{Ca} channels, and SMC hyperpolarization in human and porcine RA-IMCAs

Bradykinin increased cytoplasmic Ca^{2+} in endothelial cells of myogenically constricting, pressurized RA-IMCAs. Human IMCAs were less sensitive than porcine arteries, with a threshold around 10 nM to initiate Ca^{2+} waves in *circa* 50% of cells, which appeared to be a maximum effect as no further increase followed 100 nM (Figures 5A,C,D).

In contrast, in porcine IMCAs, 0.1 nM bradykinin initiated Ca^{2+} events in 50% of cells, rising to include all cells with 1 nM bradykinin (Figures 5B,E,F). The ability of low nM bradykinin to evoke EC Ca^{2+} events correlated with the greater sensitivity of vasodilation observed in porcine compared to human arteries (Figure 1). ECs in both species showed discrete immunolabelling for both $\text{K}_{\text{Ca}3.1}$ and $\text{K}_{\text{Ca}2.3}$, respectively the intermediate- and small-conductance K_{Ca} channels responsible for endothelium-dependent hyperpolarization (EDH; Figures 6A,B). The expression of $\text{K}_{\text{Ca}3.1}$ was consistent



and abundant in ECs of both species. In contrast, the expression of $\text{K}_{\text{Ca}2.3}$ although abundant in porcine ECs was less evident in ECs of human IMCAs, with some punctate label detected in the SMCs. Bradykinin has been shown previously to stimulate SMC hyperpolarization in human RA-IMCAs pre-constricted with endothelin-1 (12). Here, porcine RA-IMCAs pre-constricted with the thromboxane mimetic U46619 (0.6 μM) under isometric conditions were exposed to 10 nM bradykinin, which stimulated 17.3 ± 4.1 mV hyperpolarization (initial resting potential -52.6 ± 0.6 mV, with U4: -43.7 ± 1.2 mV, $n = 3$; Figures 6C,D), and completely reversed U46619 pre-constriction. Bradykinin also hyperpolarized a porcine RA-IMCA with myogenic tone, 10 nM bradykinin fully reversing tone and maximally hyperpolarizing the artery (Figure 6E).

Vasodilation to bradykinin is mediated by EDH not NO in human and porcine RA-IMCAs

Block of NO synthase with L-NAME did not modify bradykinin-mediated vasodilation in either human (Figure 7A) or porcine IMCAs (Figure 7C), whereas raising extracellular K^+ to block hyperpolarization effectively abolished responses to bradykinin. In the presence of L-NAME, the K_{Ca} subtype activated by bradykinin was probed with specific blocking agents. Vasodilation was significantly reduced in both species by exposure to a combination of TRAM-34 and apamin consistent with the known role of these channels in mediating EDH across a wide range of species. Iberiotoxin, which acts specifically to block SMC BK_{Ca} channels was without effect (Figures 7B,D).

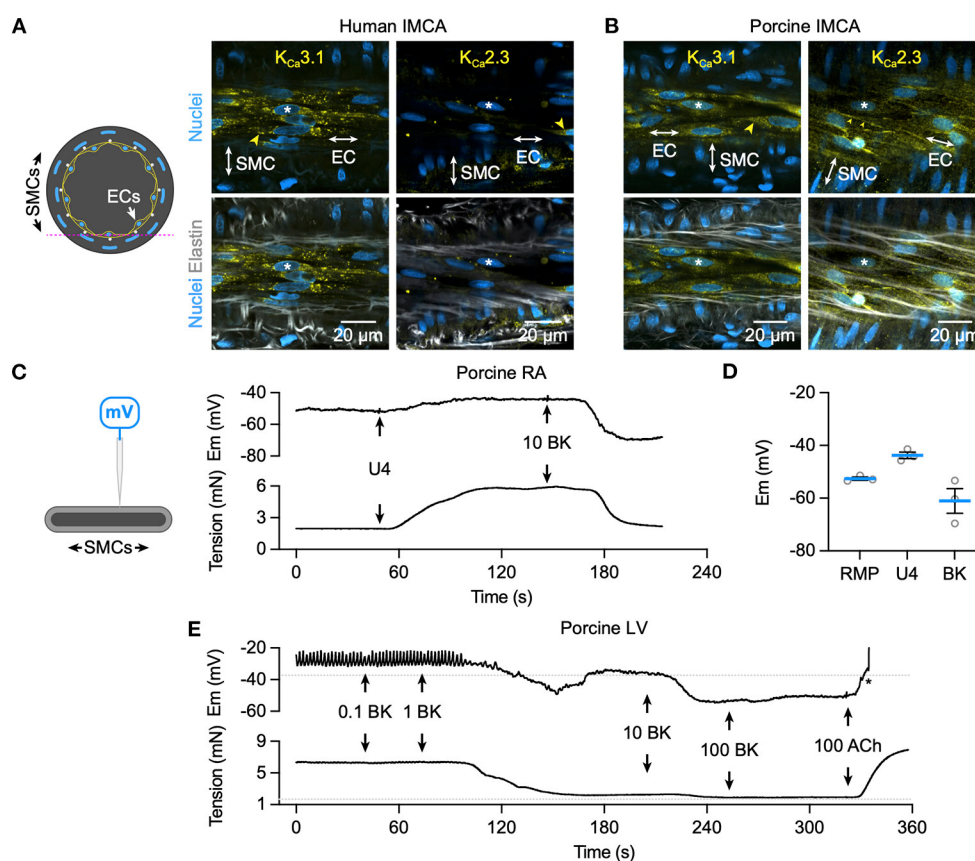


FIGURE 6

K^+ channel expression and hyperpolarization to bradykinin in human and porcine IMCAs. Confocal micrographs of immunolabelling for $K_{Ca3.1}$ and $K_{Ca2.3}$ in isolated, cannulated and pressurized human (A) and porcine (B) RA-IMCAs with myogenic tone and full dilation to BK. Punctate and diffuse $K_{Ca3.1}$ label was evident in the ECs of human and porcine arteries, whereas $K_{Ca2.3}$ was less clear in human IMCAs, and highly expressed at EC borders of porcine IMCAs (yellow arrowheads). The elastin was dense in human arteries, with the internal elastic lamina (IEL) seen as longitudinal strings in the porcine arteries. Representative of at least 3 arteries for each label; asterisks indicate corresponding nuclei in upper and lower panels. The pink dashed line in the schematic represents the focal plane. (C) The schematic indicates a sharp microelectrode impaled into a SMC of a porcine RA-IMCA mounted for isometric tension recording. Under control conditions the thromboxane mimetic U46619 (0.6 μ M) depolarized and contracted arteries, and BK (10 nM) caused hyperpolarization and relaxation (C), summarized in (D). (E) Addition of L-NAME depolarized and contracted porcine left ventricular (LV)-IMCAs. Under these conditions BK (0.1 nM to 100 nM) repolarized and relaxed the artery. Addition of 100 nM acetylcholine (ACh) depolarized and contracted the artery. The asterisk indicates when the electrode came out of the cell. The RMP and tension prior to the addition of L-NAME (100 μ M) are indicated by dashed lines. Drugs were added to a static bath at the arrows. RMP, resting membrane potential.

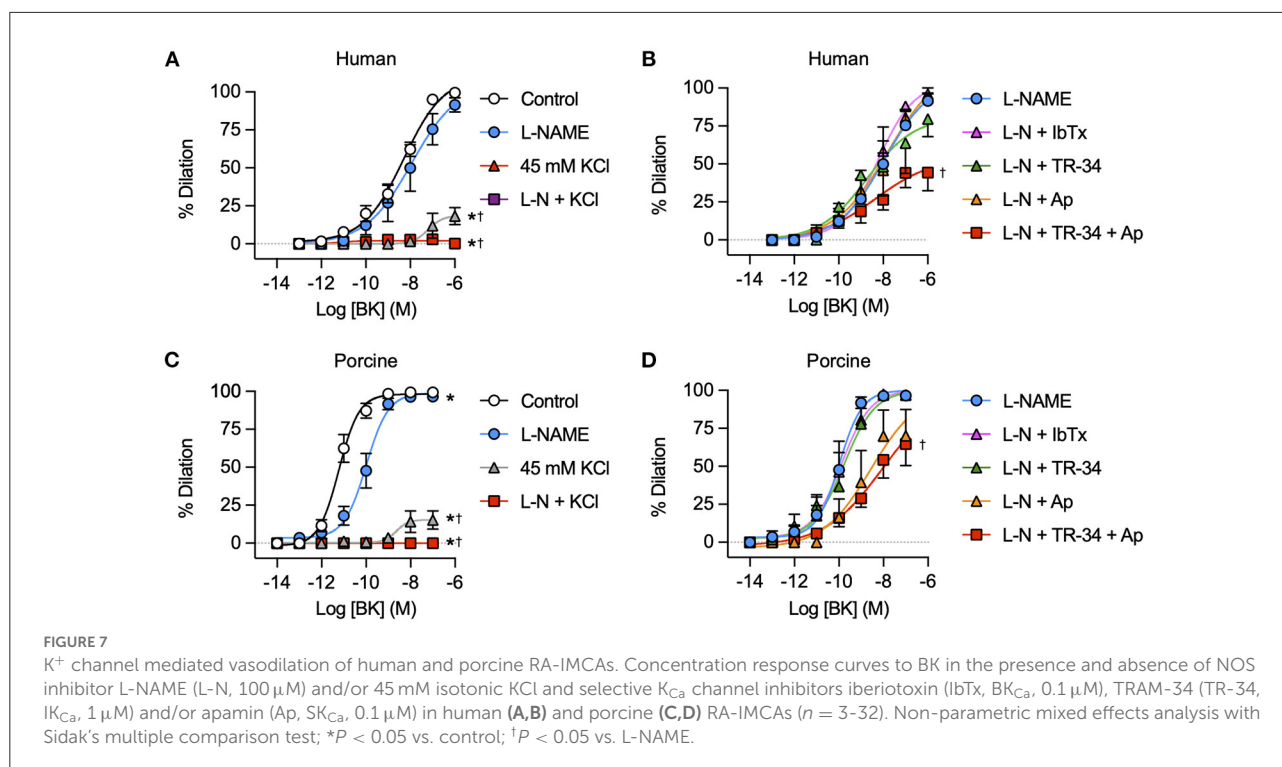
Vasodilation to adenosine is mediated by hyperpolarization in porcine RA-IMCAs

For comparison to bradykinin, the partially endothelium-dependent coronary vasodilator adenosine (29) was used to study local and conducted vasodilation in porcine RA-IMCAs. The experimental approach was the same as for bradykinin (Figure 8A), and concentration-dependent vasodilation was observed (Figure 8B), with $EC_{50} \sim 0.1 \mu$ M. Conducted vasodilation to adenosine was robust in the porcine RA-IMCAs and blocked in the combined presence of Ba^{2+} and glibenclamide (to inhibits K_{ATP} channels). Individually, these agents only partially inhibited vasodilation, while raised extracellular K^+ blocked local and conducted dilation

(Figure 8C). Adenosine stimulated concentration-dependent hyperpolarization, which was associated with relaxation (Figure 8D).

l-SMCs and r-SMCs are coupled

The l-SMCs in the wall of human and porcine RA-IMCAs (Figure 2) (18) have not been fully characterized in terms of their physiological role. Their orientation and intercellular homo- and heterocellular contacts lends them to facilitating the passage of current through the wall of coronary IMCAs. We have previously shown that SMCs in rat septal intramuscular (coronary) arteries exhibit T-type and L-type VGCC-dependent



transient depolarizing spikes which are driven once a threshold depolarization is surpassed (26). The presence of I-SMCs was confirmed by immunolabel (Figures 9A,B) and the coupling between r-SMCs and I-SMCs was demonstrated as synchronous Ca²⁺ flashes in both cell types (Figure 9C).

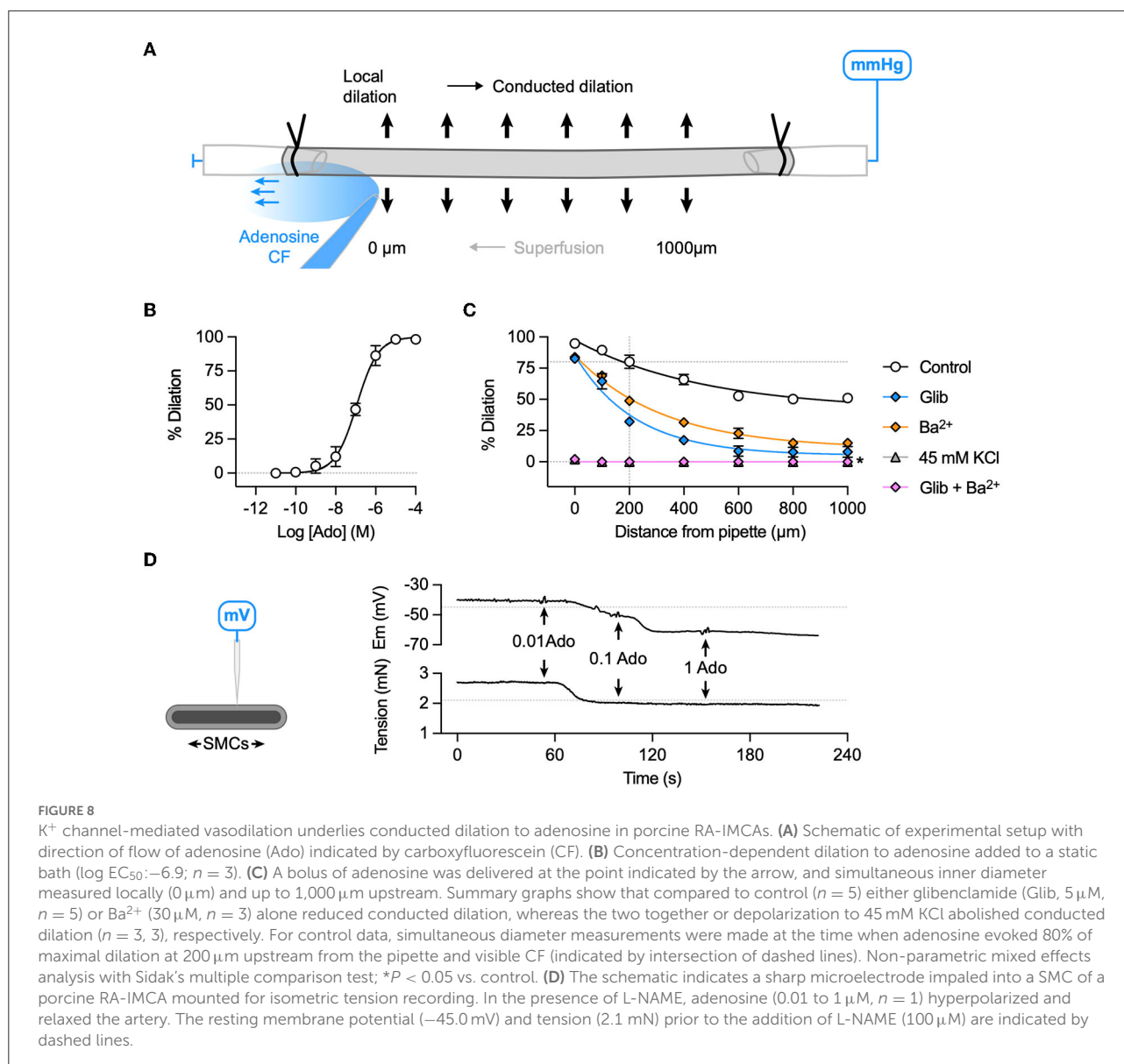
Structural observations in coronary micro-arteries with contractile dysfunction

The re-constructed 3D-structure of coronary arteries with contractile dysfunction showed that despite poor contractile function the ECs made multiple contacts with I-SMCs and r-SMCs, filling the gaps between the dense collagen and elastin present in the arterial wall (Figures 10–12). Artery #2 (Table 2) developed <10% MT, yet conducted dilation could still be observed in response to focally applied bradykinin (Figure 10). Artery #3 (Table 2) did not develop myogenic tone, hence conducted dilation could not be assessed. Nevertheless, it was striking that when cells were observed as single images in a xy-axis focal plane (Figure 11B), the cells did not appear to contact each other, yet when they were reconstructed in the z-axis, it was clear that each cell made multiple intercellular contacts, both homo- and heterocellular (Figures 10–12), highlighting the importance of this reconstruction in formulating the architecture of arteries.

Discussion

The current study reveals a remarkably similar profile of vasodilation to bradykinin in myogenically-active human and porcine intramyocardial arteries. IMCAs were isolated from either atria or ventricle, with access to organ donor biopsies providing a rare opportunity to study human left ventricular IMCAs. The only notable difference between the human and porcine vessels was the potency of bradykinin. We also show importantly that myogenically contracting human and porcine IMCAs can develop robust conducted vasodilation following restricted application of either bradykinin or in porcine IMCAs to adenosine, and that the underlying cellular mechanism varies with each autacoid. Bradykinin generated hyperpolarization and vasodilation by activating EC K_{Ca} channels, with apparent no input from either NO or K_{IR} channels, while adenosine vasodilation relied on activation of both K_{ATP} and K_{IR} channels. Overall, our data support the ongoing use of right atrial appendage biopsies from patients and from pigs undergoing cardiopulmonary surgery as a useful model of human IMCAs.

Any dilator agonist or autacoid able to stimulate local vascular hyperpolarization will potentially also initiate conducted vasodilation (30, 31), depending on extensive gap-junction coupling, to allow hyperpolarization to spread axially along the arterial endothelium (31–33). The hyperpolarizing current spreads radially to the smooth muscle layers via heterocellular myoendothelial gap junctions, with the resulting



hyperpolarization causing vasodilation by reducing the open-probability of voltage-gated calcium channels (8, 9). The spread of hyperpolarization along the endothelium appears to be facilitated, as the length constant is greater than expected for a purely passive process (34). Whether this reflects a difference in the duration of hyperpolarizing stimulus or an additional facilitating mechanism is not clear. However, one suggestion is that this facilitation is at least in part due to the activity of vascular K_{IR} channels (11), but there are likely other as yet undefined processes to consider.

The endothelium usually expresses two forms of K_{Ca} channel, of small (SK_{Ca}) and intermediate (IK_{Ca}) conductance, that are activated by any agonist/autocoid that increases EC

cytoplasmic calcium. This distribution contrasts with the large conductance K_{Ca} channels (BK_{Ca} channels), usually confined to SMCs. Bradykinin-evoked vasodilation in human coronary arterioles precontracted with endothelin appears to be entirely due to hyperpolarization generated by activation of K_{Ca} channels, without any significant contribution from either nitric oxide or cyclooxygenase derivatives (12). In both human and porcine coronary IMCAs this endothelium-dependent hyperpolarization may reflect the release of H₂O₂ and/or epoxyeicosatrienoic acids activating SMC BK_{Ca} channels (12, 35–37). However, in human coronary IMCAs precontracted with the thromboxane-mimetic U46619, bradykinin-evoked vasorelaxation is due to hyperpolarization generated solely by EC SK_{Ca} and IK_{Ca} channel activity and by the release

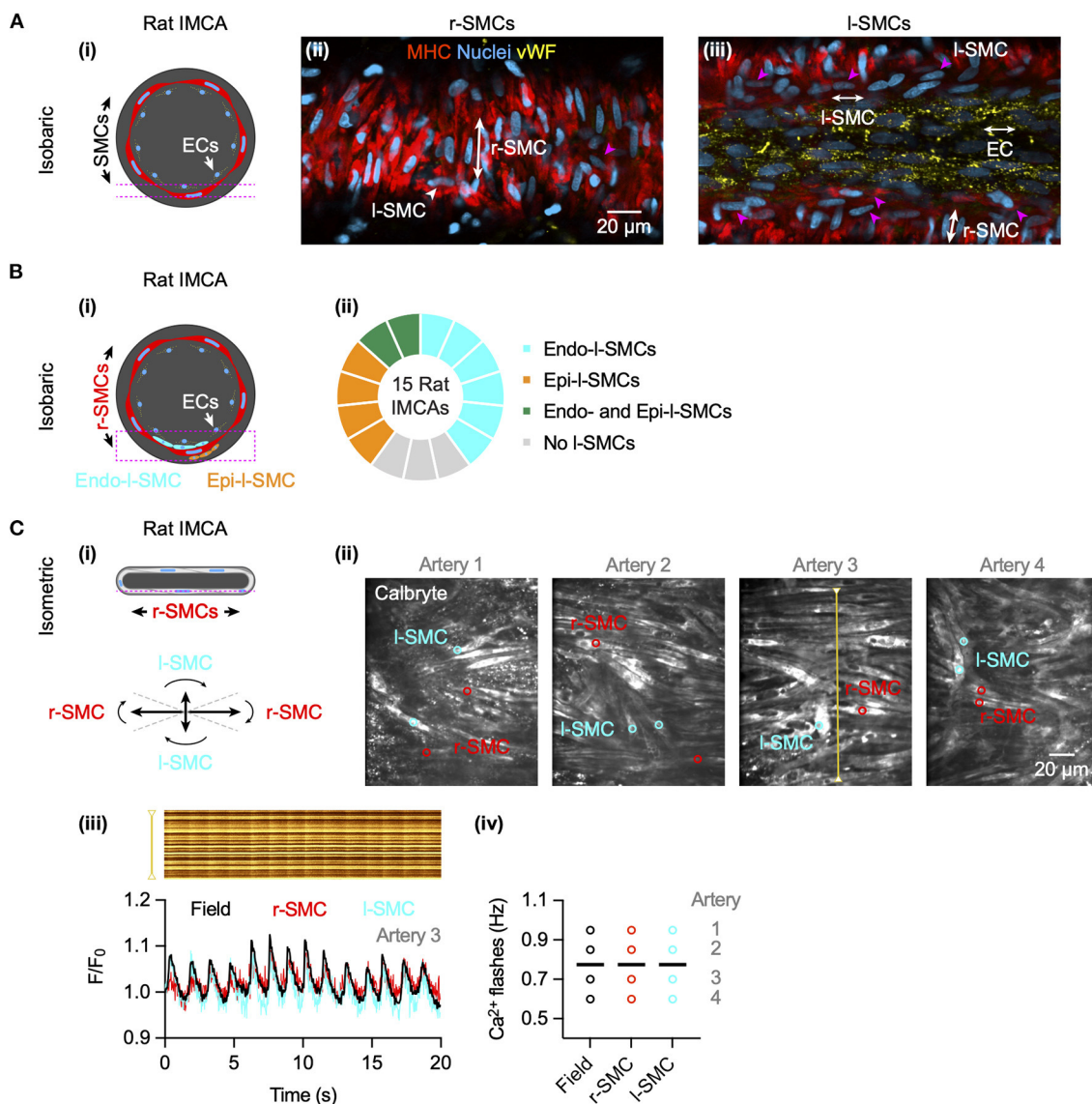
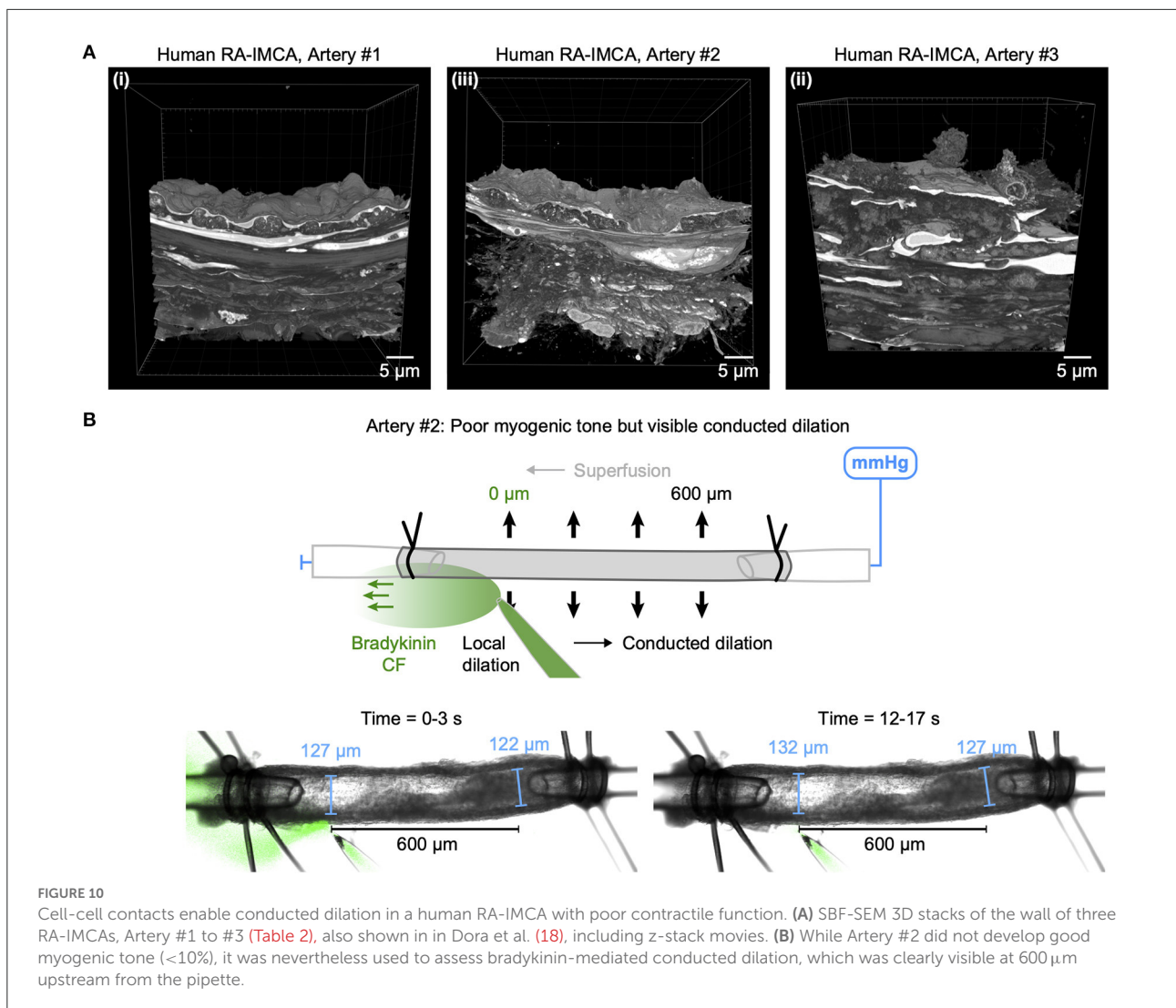


FIGURE 9

Cell-cell contacts facilitate electrical communication in coronary arteries. **(A)** Rat septal IMCAs each developed myogenic tone when mounted for pressure myography ($25.1 \pm 2.8\%$, $n = 15$). Arteries were fixed and immunolabelled for SM-myosin heavy chain II to label SMCs and von Willebrand factor (vWF) for ECs. Both r-SMC and I-SMCs were visible, the latter clearly separate from ECs. The pink dashed lines in the schematic **(i)** show the focal planes for imaging the SMCs **(ii)** and ECs **(iii)** of the same artery. Pink arrowheads show examples of I-SMCs. Representative of 12 arteries (of 15 imaged) with I-SMCs. **(B)** In pressurized arteries **(i)**, I-SMCs were observed between the ECs and r-SMCs (endo-I-SMCs) and outside the r-SMCs (epi-I-SMCs). **(ii)** Most arteries had endo-I-SMCs (12 of 15), and some had both endo-I-SMCs and epi-I-SMCs (2 of 15). 3 arteries had <5 I-SMCs in the z-stack (region indicated by dashed pink box in **(i)**), considered no I-SMCs. **(C)** In arteries set up in a confocal wire myography **(i)** SMCs were imaged at the bottom surface (focal plane indicated by dashed pink line). The r-SMCs were often in the same focal plane as the I-SMCs (angles for categorization shown). **(ii)** Confocal micrographs of 4 arteries are shown with regions used for average fluorescence (indicated by colored circles). **(iii)** The spatio-temporal characteristics of spontaneous SMC Ca²⁺ flashes in Artery 3 are shown in line-scan analysis of the yellow line (upper), and corresponding average fluorescence intensity within a r-SMC (red) and I-SMC (cyan) and the whole field (black) as F/F₀ below. Summary data are shown in **(iv)**, each individual artery had simultaneous Ca²⁺ flashes within all r-SMCs and I-SMCs, the frequency only varying between arteries (mean indicated by bars; 0.78 ± 0.08 Hz, $n = 4$).

of NO (13). This finding was based on the ability of a specific SK_{Ca} blocker apamin combined with charybdotoxin (which blocks both intermediate- and large-conductance K_{Ca} channels, IK_{Ca} and BK_{Ca}) and the NO scavenger

hydroxocobalamin to markedly inhibit vasodilation. However, substituting charybdotoxin with a specific BK_{Ca} blocker, iberiotoxin failed to modify vasodilation (13). Our data were obtained in IMCAs during spontaneous myogenic constriction,



with no need for agonist-evoked vasoconstriction. Although bradykinin evoked both local and conducted vasodilation through hyperpolarization, this was predominantly due to activation of EC SK_{Ca} and IK_{Ca} channels, as it was abolished either by raised extracellular potassium, or much reduced by the selective K_{Ca} blockers, apamin with TRAM-34, consistent with data from other groups (10, 12) (summarized in Table 3). In addition, we now show these K_{Ca} channel proteins are expressed and localized within both human and porcine IMCAs ECs, as in other species. Lack of inhibition with iberiotoxin indicates there is not a predominant role for BK_{Ca} in bradykinin vasodilation against myogenic tone, in arteries with myogenic tone matched to those of healthy pigs (18). Although these data contrast with previous observations, they may be reconciled by the finding that myoendothelial cell-cell contacts decline as microvascular dysfunction develops (18), perhaps secondary to large coronary artery disease (note the previous use of CABG

surgery patients) (10, 12). In the latter studies the arteries may adapt to rely more on a diffusible endothelial factor acting to stimulate vasodilation via SMC BK_{Ca} channels. SK_{Ca} and IK_{Ca} together generate endothelium-dependent hyperpolarization, which is the primary endothelial vasodilator mechanism in many small arteries (9). Interestingly, some vasodilation did persist after block of EDH (combined block of SK_{Ca} and IK_{Ca} during NO synthesis block with L-NAME), but was abolished by raised extracellular K⁺, which may indicate input from an as yet unidentified potassium conductance. Whether this residual vasodilation to bradykinin in myogenically-active porcine and human atrial intra-pectinate arteries is in any way reliant on EC cytochrome P450 mono-oxygenase, and possibly BK_{Ca} channels, as suggested in ventricular subepicardial arterioles (35), remains to be established.

There has been only one previous report of conducted vasodilation in human RA coronary arteries during myogenic

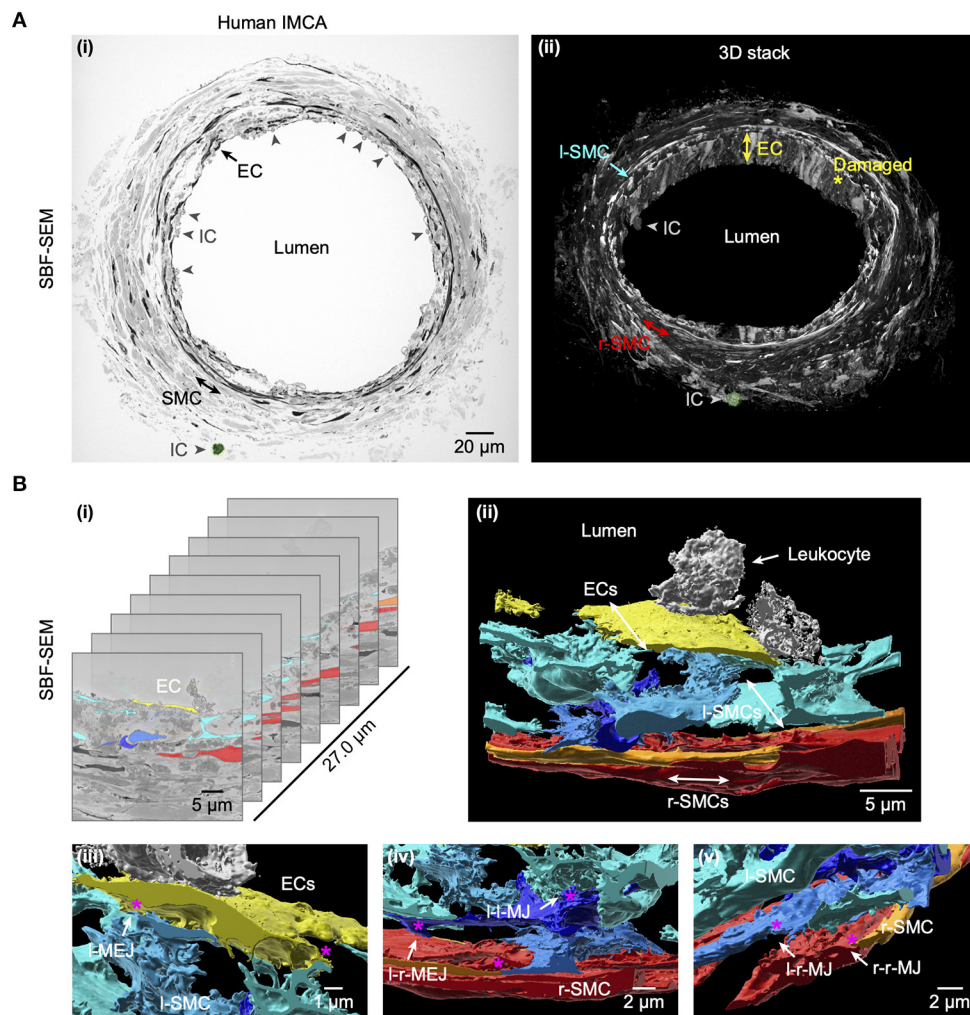


FIGURE 11

Cell-cell contact sites in a human RA-IMCA with contractile dysfunction. The artery (Artery #3, Table 2) did not develop myogenic tone but was processed for serial block face scanning electron microscopy. At low resolution (A) it is clear that many ECs are damaged and inflammatory cells (ICs) have adhered to the artery wall, the same IC is highlighted in green in both the 2D- (left) and 3D- (right) images. A movie through the 3D z-stack at low and higher resolution is available at Dora et al. (18). (B) The cell-cell contact sites were visible in the SBF-SEM images. Individual cells were 3D rendered and are shown superimposed on the original images (i) and as the reconstructed artery walls (ii–v; Supplementary Video 4). Multiple layers of interspersed longitudinally arranged SMCs (l-SMCs) are shown in blue (see also Figure 12), and circumferential radial SMCs (r-SMCs) in orange and red; each of which contacted each other and often adjacent endothelial cells. Examples are indicated by r-MEJ, r-SMC to EC junction; l-MEJ, l-SMC to EC junction; l-l-MJ, l-SMC to l-SMC junction; r-r-MJ, r-SMC to r-SMC junction.

vasoconstriction and this also indicated a central role for SK_{Ca} and IK_{Ca} channels during bradykinin stimulation (10). Furthermore, this study showed that conducted vasodilation to bradykinin was abolished by the gap junction uncouplers, carbenoxolone or 18α -glycyrrhetic acid, neither of which altered local vasodilation. Interestingly, NO was proposed to facilitate the passage of hyperpolarizing current along the endothelium, as the vasodilation 500 μm upstream from the bradykinin delivery pipette was sensitive to block of NO synthase even though K_{Ca} channels were still available (10). The authors also showed that conducted vasodilation was less in

arteries from older (>64 years) compared to younger patients, suggesting an age-linked decrease in NO bioavailability might be responsible (10) (Table 3). This was the first time NO had been implicated directly in conducted vasodilation, as previous studies with skeletal muscle had discounted the possibility (40). Our data do not support a predominant role for NO in either local or conducted vasodilation in human or pig IMCAs. One possible explanation for these differences may relate to the type of patient recruited. Biopsies came from patients with established coronary artery disease (26 of 30 patients undergoing CABG surgery) in the study by Feher et al. (10) whereas only 3

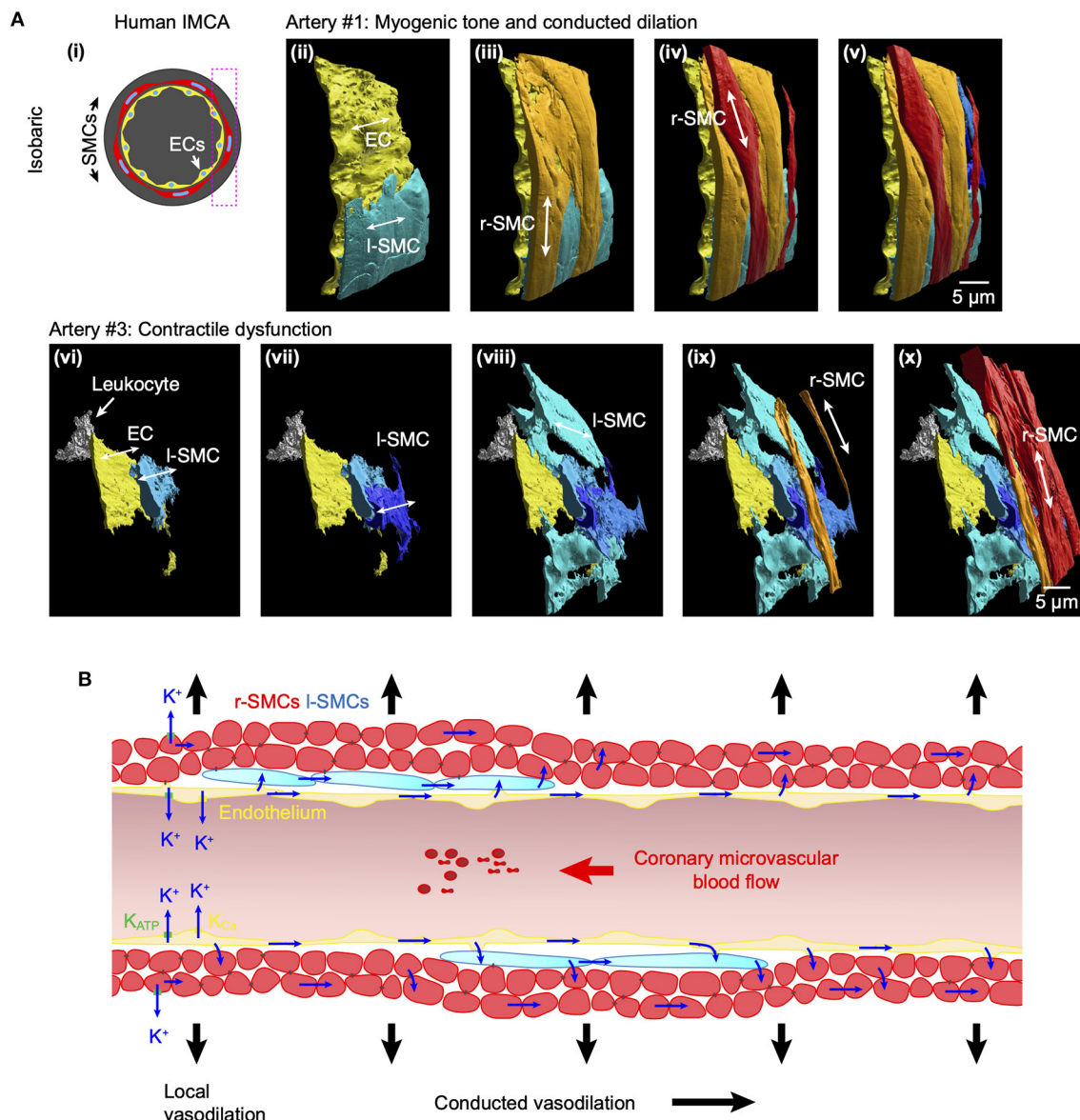


FIGURE 12 Arrangement of SMCs in human RA-IMCAs with and without contractile function. **(A)** Not all human IMCAs developed myogenic tone, but cell-cell contacts were always visible between ECs, r-SMCs and I-SMCs. Pressurized human IMCAs (i) were fixed and processed for SBF-SEM. Artery #1 is shown here from the rear, with sequence of added cell types (ii–v). Artery #3 did not develop myogenic tone, had missing ECs and was fibrotic. Despite this, ECs made contact with I-SMCs, many of which made contact with each other and then ultimately the r-SMCs in the outer surface (vi–x). An inflammatory cell (leukocyte) is attached to the endothelium. **(B)** Schematic of conduction pathways in coronary IMCAs. In human, porcine and rat IMCAs I-SMCs are found between the endothelium and circumferentially-orientated radial r-SMCs. The I-SMCs provide an additional pathway for intercellular communication and, where gap junctions are present, will facilitate conducted dilation.

CABG patients were included in our present study, and none of these biopsies were used to in experiments to measure conducted vasodilation. This patient-specific difference clearly warrants further investigation, as it has potential implications for the control of blood flow within the microcirculation of patients with epicardial coronary artery inflammation, intimal plaque formation and microvascular ischaemia. It also suggests that

arterial function may be better preserved in patients undergoing valve surgery. By extension, our study supports the use of the porcine-derived samples as a model for healthy human arteries. Our high resolution microscopy also shows endothelial and smooth muscle cell contacts in RA-IMCAs, supporting the previous functional assessment using gap-junction uncouplers (10). Whether functional myoendothelial contacts remain in

TABLE 3 Summary of some key published responses to bradykinin in human IMCAs.

Source of arteries	Diameter (μm)	Pressure (mmHg)	Tone	Mechanism of dilation	References
RA-Endo; LV- Endo/Epi	103 \pm 2 (RA); 148 \pm 10 (LV)	60	MT or ET-1	Not explored; LV data not shown	(38)
RA	97 \pm 4	60	ET-1	BK _{Ca} - and SK _{Ca} -mediated hyperpolarisation	(12)
Branch off LAD	160–600; mean 380	100 (WM)	U46619	NO, K _{IR} , Na ⁺ /K ⁺ ATPase; IK _{Ca} and SK _{Ca}	(13)
RA	158 \pm 6	60	ACh or ET-1	Superoxide and H ₂ O ₂ production	(37)
RA	124 \pm 8	80	MT	Conducted dilation: Gap junction-dependent, IK _{Ca} and SK _{Ca} ; NO in young (<64 y) subjects	(10)
Parietal pericardium	187 \pm 4	100 (WM)	K ⁺ , U46619, ET-1	Agonist dependent; NO for K ⁺ and U46619, H ₂ O ₂ for ET-1	(39)
RA-Endo LV-Endo	153 \pm 6	80	MT	EC Ca ²⁺ -dependent activation of IK _{Ca} and SK _{Ca}	*

Endo, endocardial surface; Epi-epicardial surface; WM, wire myograph (isometric tension); MT, myogenic tone; ET-1, endothelin-1; ACh, acetylcholine; *, current study.

the arterioles from CABG surgery patients, and how NO might influence electrical coupling and current spread are clearly areas that merit further investigation. It seems unsurprising that with age and large coronary artery disease multiple mechanisms may contribute to disrupt coronary microvascular blood flow.

The conducted dilation to bradykinin was not affected by low micromolar Ba²⁺ in both human and porcine RA-IMCAs, arguing against a role for K_{IR} channels in either local or conducted vasodilation. Notably, Ba²⁺ visibly contracted each artery suggesting a functional activation of K_{IR} channels during myogenic tone. In contrast a previous study using porcine coronary arterioles (50–110 μm) suggested a significant functional role for K_{IR} channels in bradykinin-mediated vasodilation (11). These divergent observations may reflect the source for the arteries. We isolated intra-pectinate arteries, while the earlier study used branches of the left anterior descending and circumflex epicardial arteries (11, 41). Our data are in accordance with the concentration-dependent vasodilation to

bradykinin in the ventricular biopsies, with an EC₅₀ near 0.1 nM (11).

While responses to bradykinin are useful to show the importance of the endothelium, clinically the assessment of coronary flow reserve usually follows an infusion of adenosine, which serves as a good indicator of vasodilator capacity within the heart. Adenosine is usually released during coronary metabolic stress and stimulates coronary vasodilation *via* both endothelial and smooth muscle receptors. We compared the ability of adenosine to evoke conducted vasodilation to bradykinin. Our data confirm a role for glibenclamide-sensitive K_{ATP} channels in adenosine-evoked vasodilation of porcine coronary arterioles, channels that are expressed in both EC and SMC cells in subepicardial arterioles (29, 42–44). The endothelium-dependent component of vasodilation in porcine coronary arterioles has been shown to rely on NO release (29, 42, 43) *via* a pertussis toxin-sensitive pathway (42). This sensitivity suggests G_{i/o}-coupling, and as both A₁ and A₃ receptors are G_{i/o} linked, either or both may be expressed on ECs and cause

NO release. Furthermore, smooth muscle-dependent dilation to adenosine was fully blocked by glibenclamide (but not pertussis toxin) (42), supporting a direct role for the G_s -coupled A_{2A} receptors causing vasodilation following hyperpolarization of SMCs (42). In contrast, studies in large porcine coronary arteries have failed to reduce adenosine-mediated vasodilation with glibenclamide (45). Furthermore, while adenosine evokes robust dilation in human RA-IMCAs studied *ex vivo* (46, 47), it was neither endothelium-dependent (47) nor sensitive to glibenclamide (46). This can be explained by variation in the signaling pathways downstream of the adenosine receptor subtypes across species and arteriolar diameters. Of relevance here is that other K^+ channels have also been suggested to play a role in adenosine-mediated porcine coronary artery dilation, including K_{IR} channels (11) and K_{v7} channels (48). Clearly, the mechanisms that underly adenosine-mediated vasodilation in both the porcine and human coronary microvasculature requires further characterization.

An important consideration in the coronary microcirculation is the unusual presence of l-SMCs between the endothelium and r-SMCs. These cells were observed in human and porcine atrial and ventricular IMCAs (18) and now in rat septal intramuscular arteries. While the cells appear to have a synthetic phenotype in healthy arteries, they change to a more contractile phenotype in human RA-IMCAs with contractile dysfunction (18). The extensive homo- and heterocellular cell-cell contacts between ECs and l-SMCs and also from l-SMCs to r-SMCs in human RA-IMCAs with and without contractile dysfunction suggests a novel physiological role for l-SMCs: facilitating the spread of current and potentially chemical signals between cells, either *via* gap junctions or by the diffusion of released factors. While we cannot point to which pathways operate, there is evidence that gap junction uncouplers block conducted dilation in human RA-IMCAs (10), and that electrical coupling enables action potential-like spikes dependent on VGCCs in small arteries (49). Here we show that in rat septal arteries these depolarizing spikes (26) are associated with Ca^{2+} flashes that are synchronous between all the SMCs in a field of view, both l-SMCs and r-SMCs. This strongly supports electrical coupling as a signaling mechanism between the SMCs, and raises the intriguing possibility that l-SMCs support the crucial role of ECs in propagating signals upstream to evoke conducted dilation (32) in the coronary microcirculation (Figure 12B).

Study limitations

A major limitation to understanding how the coronary microcirculation works is not being able to establish the contribution of conducted dilation to the control of coronary blood flow *in vivo*. While it has been shown that both bradykinin and adenosine are vasodilators in the coronary microcirculation *in vivo* (50), it is not possible to pinpoint the release or

delivery of each agonist to assess the extent of electrical coupling in influencing upstream artery diameter. Furthermore, flow-induced dilation may contribute alongside conducted dilation, particularly in the larger diameter arteries. Therefore, responses must be studied under controlled conditions *ex vivo*. In the present study, a lack of tissue availability means we have been unable to establish whether conducted vasodilation is significant in human (or pig) ventricle-derived IMCAs. This aspect warrants future investigation. Future *ex vivo* studies should be extended to disease models, including porcine models of acute myocardial infarction and ischaemia and non-obstructive coronary artery disease, as steps toward understanding the operation and failing of the human coronary microcirculation (6).

Conclusions

Our data demonstrate that intramyocardial arteries from the atria and ventricles of pigs and organ donors can be used for *ex vivo* studies of microvascular function. Obtaining access to viable ventricular biopsies is extremely difficult, so our *ex vivo* data showing responses to the EC-dependent dilator bradykinin have the same profile across species and heart chambers is an important step forward. Once vasodilation was initiated by focal application of bradykinin or adenosine in IMCAs, it spread with minimal decline along the entire length of these small coronary arteries, secondary to hyperpolarization.

Data availability statement

The raw data supporting the conclusions of this article will be made available by the authors, without undue reservation.

Ethics statement

The studies involving human participants were reviewed and approved by Oxford Research Ethics Committee. The patients/participants provided their written informed consent to participate in this study. The animal study was reviewed and approved by University of Bristol Research Ethics and University of Oxford Ethical Committee.

Author contributions

KD conceived and designed the experiments, collected and analyzed data, prepared the figures, and wrote the manuscript. JL, LB, TB, and CG collected and analyzed data. KD and JL performed the statistical analysis. RA and MT provided human and porcine specimens, and contributed to manuscript preparation. KD, JL, LB, TB, MT, RA, and CG proof-read the manuscript. All authors contributed to the article and approved the submitted version.

Funding

This work was supported by the British Heart Foundation (BHF) and Medical Research Council (MRC) Grants to RA [Grant Numbers BHF: PG/18/49/33833, IG/14/2/30991, PG/16/104/32652, and MRC MR/L012723/1] and by the Bristol NIHR Biomedical Research Center. Organ Donor Heart Collection was funded by the NIHR Cambridge/Newcastle Blood and Transplant Research Unit (BTRU). In addition, this work was supported by British Heart Foundation Grants to KD [Grant Numbers FS/08/033/25111, FS/13/16/30199, IG/13/5/30431, PG/18/11/33552, and PG/20/10260] and by the Oxford BHF Centre of Research Excellence [Grant Number RE/13/1/30181].

Acknowledgments

We thank the research nurses, lab technicians and surgeons at the Bristol Heart Institute, University Hospital NHS Foundation Trust, Bristol Trials Centre (Clinical Trials and Evaluation Unit) at the University of Bristol, and the staff at the University of Bristol Translational Biomedical Research Centre, a national research facility for large animals co-funded by the BHF and MRC. We appreciate the assistance of Prof. John Dark, Dr. Lu Wang, and Lucy Bates (Newcastle) in organ retrieval and biopsy provision. We express our full gratitude to all the patients taking part in this study. Finally we thank Dr. Lauren Phillips for her guidance regarding 3D rendering of the arteries.

Conflict of interest

The authors declare that the research was conducted in the absence of any commercial or financial relationships that could be construed as a potential conflict of interest.

References

- Jones CJ, Kuo L, Davis MJ, Chilian WM. Regulation of coronary blood flow: coordination of heterogeneous control mechanisms in vascular microdomains. *Cardiovasc Res.* (1995) 29:585–96. doi: 10.1016/S0008-6363(96)88626-3
- Duncker DJ, Koller A, Merkus D, Cauty JM Jr. Regulation of coronary blood flow in health and ischemic heart disease. *Prog Cardiovasc Dis.* (2015) 57:409–22. doi: 10.1016/j.pcad.2014.12.002
- Zhang Z, Takarada S, Molloy S. Assessment of coronary microcirculation in a swine animal model. *Am J Physiol Heart Circ Physiol.* (2011) 301:H402–8. doi: 10.1152/ajpheart.00213.2011
- Wong JT, Molloy S. Determination of fractional flow reserve (FFR) based on scaling laws: a simulation study. *Phys Med Biol.* (2008) 53:3995–4011. doi: 10.1088/0031-9155/53/14/017
- Wong JT, Le H, Suh WM, Chalyan DA, Mehraien T, Kern MJ, et al. Quantification of fractional flow reserve based on angiographic image data. *Int J Cardiovasc Imaging.* (2012) 28:13–22. doi: 10.1007/s10554-010-9767-0
- Pries AR, Reglin B. Coronary microcirculatory pathophysiology: can we afford it to remain a black box? *Eur Heart J.* (2017) 38:478–88. doi: 10.1093/eurheartj/ehv760
- Hilton SM. A peripheral arterial conducting mechanism underlying dilatation of the femoral artery and concerned in functional vasodilatation in skeletal muscle. *J Physiol.* (1959) 149:93–111. doi: 10.1113/jphysiol.1959.sp006327
- Segal SS. Integration and modulation of intercellular signaling underlying blood flow control. *J Vasc Res.* (2015) 52:136–57. doi: 10.1159/000439112
- Garland CJ, Dora KA, EDH. endothelium-dependent hyperpolarization and microvascular signaling. *Acta Physiol.* (2017) 219:152–61. doi: 10.1111/apha.12649

Publisher's note

All claims expressed in this article are solely those of the authors and do not necessarily represent those of their affiliated organizations, or those of the publisher, the editors and the reviewers. Any product that may be evaluated in this article, or claim that may be made by its manufacturer, is not guaranteed or endorsed by the publisher.

Supplementary material

The Supplementary Material for this article can be found online at: <https://www.frontiersin.org/articles/10.3389/fcvm.2022.980628/full#supplementary-material>

SUPPLEMENTARY VIDEO 1

3D render of cells in the wall of an isolated, cannulated and pressurized human RA-IMCA human with myogenic tone and conducted dilation to bradykinin, Artery #1. Refer to **Figures 2, 10A, 12A** for details; ECs yellow, l-SMC shades of blue, r-SMCs shades of red/orange.

SUPPLEMENTARY VIDEO 2

Local and conducted dilation to bradykinin in a human RA-IMCA. Top: Simultaneous transmitted and fluorescence images. Bottom: Fluorescence images showing the autofluorescence of the elastin along the artery, along with the delivery of bradykinin. The corresponding time course is shown in **Figure 3**.

SUPPLEMENTARY VIDEO 3

Local and conducted dilation to bradykinin in a porcine RA-IMCA. Top: Simultaneous transmitted and fluorescence images. Bottom: Fluorescence images showing the delivery of bradykinin, the only visible fluorescence. The corresponding time course is shown in **Figure 3**.

SUPPLEMENTARY VIDEO 4

3D render of cells in the wall of an isolated, cannulated and pressurized human RA-IMCA with no myogenic tone, Artery #3. Refer to **Figures 10A, 11, 12A** for details; ECs yellow, l-SMC shades of blue, r-SMCs shades of red/orange, leukocytes white.

10. Feher A, Broskova Z, Bagi Z. Age-related impairment of conducted dilation in human coronary arterioles. *Am J Physiol Heart Circ Physiol.* (2014) 306:H1595–601. doi: 10.1152/ajpheart.00179.2014
11. Rivers RJ, Hein TW, Zhang C, Kuo L. Activation of barium-sensitive inward rectifier potassium channels mediates remote dilation of coronary arterioles. *Circulation.* (2001) 104:1749–53. doi: 10.1161/hc4001.098053
12. Miura H, Liu Y, Gutterman DD. Human coronary arteriolar dilation to bradykinin depends on membrane hyperpolarization: contribution of nitric oxide and Ca²⁺-activated K⁺ channels. *Circulation.* (1999) 99:3132–8. doi: 10.1161/01.CIR.99.24.3132
13. Batenburg WW, Garrelts IM, van Kats JP, Saxena PR, Danser AH. Mediators of bradykinin-induced vasorelaxation in human coronary microarteries. *Hypertension.* (2004) 43:488–92. doi: 10.1161/01.HYP.0000110904.95771.26
14. Kuo L, Davis MJ, Chilian WM. Myogenic activity in isolated subepicardial and subendocardial coronary arterioles. *Am J Physiol Heart Circ Physiol.* (1988) 255:H1558–H62. doi: 10.1152/ajpheart.1988.255.6.H1558
15. Kuo L, Chilian WM, Davis MJ. Coronary arteriolar myogenic response is independent of endothelium. *Circ Res.* (1990) 66:860–6. doi: 10.1161/01.RES.66.3.860
16. Kuo L, Davis MJ, Cannon MS, Chilian WM. Pathophysiological consequences of atherosclerosis extend into the coronary microcirculation. Restoration of endothelium-dependent responses by L-arginine. *Circ Res.* (1992) 70:465–76. doi: 10.1161/01.RES.70.3.465
17. Tsang HG, Rashdan NA, Whitelaw CB, Corcoran BM, Summers KM, MacRae VE. Large animal models of cardiovascular disease. *Cell Biochem Funct.* (2016) 34:113–32. doi: 10.1002/cbf.3173
18. Dora KA, Borysova L, Ye X, Powell C, Beleznaï TZ, Stanley CP, et al. Human coronary microvascular contractile dysfunction associates with viable synthetic smooth muscle cells. *Cardiovasc Res.* (2022) 118:1978–92. doi: 10.1093/cvr/cvab218
19. Garger JC, Barbee RW, Bielitzki JT, Donovan JC, Hendriksen FM, Kohn DF, et al. *Guide for the Care and Use of Laboratory Animals: Eighth Edition.* Washington DC: National Academies Press (2011).
20. Dora KA, Stanley CP, Al Jaaly E, Fiorentino F, Ascione R, Reeves BC, et al. Isolated human pulmonary artery structure and function pre- and post-cardiopulmonary bypass surgery. *J Am Heart Assoc.* (2016) 5:1–9. doi: 10.1161/JAHA.115.002822
21. Dora KA. Conducted dilation to ATP and K⁺ in rat skeletal muscle arterioles. *Acta Physiol.* (2017) 219:202–18. doi: 10.1111/apha.12656
22. Winter P, Dora KA. Spreading dilatation to luminal perfusion of ATP and UTP in rat isolated small mesenteric arteries. *J Physiol.* (2007) 582:335–47. doi: 10.1113/jphysiol.2007.135202
23. Lemmey HAL, Ye X, Ding HC, Triggle CR, Garland CJ, Dora KA. Hyperglycaemia disrupts conducted vasodilation in the resistance vasculature of db/db mice. *Vasc Pharmacol.* (2018) 103–5:29–35. doi: 10.1016/j.vph.2018.01.002
24. Kilkenny C, Browne WJ, Cuthill IC, Emerson M, Altman DG. Improving bioscience research reporting: the ARRIVE guidelines for reporting animal research. *PLoS Biol.* (2010) 8:e1000412. doi: 10.1371/journal.pbio.1000412
25. McGrath JC, Lilley E. Implementing guidelines on reporting research using animals (ARRIVE etc): new requirements for publication in BJP. *Br J Pharmacol.* (2015) 172:3189–93. doi: 10.1111/bph.12955
26. Smith JF, Lemmey HAL, Borysova L, Hiley CR, Dora KA, Garland CJ. Endothelial nitric oxide suppresses action-potential-like transient spikes and vasospasm in small resistance arteries. *Hypertension.* (2020) 76:785–94. doi: 10.1161/HYPERTENSIONAHA.120.15491
27. Belevich I, Joensuu M, Kumar D, Vihinen H, Jokitalo E. Microscopy image browser: a platform for segmentation and analysis of multidimensional datasets. *PLoS Biol.* (2016) 14:e1002340. doi: 10.1371/journal.pbio.1002340
28. Bagher P, Beleznaï T, Kansui Y, Mitchell R, Garland CJ, Dora KA. Low intravascular pressure activates endothelial cell TRPV4 channels, local Ca²⁺ events, and IK_{Ca} channels, reducing arteriolar tone. *Proc Natl Acad Sci USA.* (2012) 109:18174–9. doi: 10.1073/pnas.1211946109
29. Kuo L, Chancellor JD. Adenosine potentiates flow-induced dilation of coronary arterioles by activating K_{ATP} channels in endothelium. *Am J Physiol Heart Circ Physiol.* (1995) 269:H541–H9. doi: 10.1152/ajpheart.1995.269.2.H541
30. Delashaw JB, Duling BR. Heterogeneity in conducted arteriolar vasomotor response is agonist dependent. *Am J Physiol Heart Circ Physiol.* (1991) 260:H1276–82. doi: 10.1152/ajpheart.1991.260.4.H1276
31. Segal SS, Duling BR. Flow control among microvessels coordinated by intercellular conduction. *Science.* (1986) 234:868–70. doi: 10.1126/science.3775368
32. Emerson GG, Segal SS. Endothelial cell pathway for conduction of hyperpolarization and vasodilation along hamster feed artery. *Circ Res.* (2000) 86:94–100. doi: 10.1161/01.RES.86.1.94
33. Takano H, Dora KA, Spitaler MM, Garland CJ. Spreading dilatation in rat mesenteric arteries associated with calcium-independent endothelial cell hyperpolarization. *J Physiol.* (2004) 556:887–903. doi: 10.1113/jphysiol.2003.06.0343
34. Emerson GG, Neild TO, Segal SS. Conduction of hyperpolarization along hamster feed arteries: augmentation by acetylcholine. *Am J Physiol Heart Circ Physiol.* (2002) 283:H102–9. doi: 10.1152/ajpheart.00038.2002
35. Hein TW, Liao JC, Kuo L. oxLDL specifically impairs endothelium-dependent, NO-mediated dilation of coronary arterioles. *Am J Physiol.* (2000) 278:H175–83. doi: 10.1152/ajpheart.2000.278.1.H175
36. Miura H, Gutterman DD. Human coronary arteriolar dilation to arachidonic acid depends on cytochrome P-450 monooxygenase and Ca²⁺-activated K⁺ channels. *Circ Res.* (1998) 83:501–7. doi: 10.1161/01.RES.83.5.501
37. Larsen BT, Gutterman DD, Sato A, Toyama K, Campbell WB, Zeldin DC, et al. Hydrogen peroxide inhibits cytochrome P450 epoxygenases: interaction between two endothelium-derived hyperpolarizing factors. *Circ Res.* (2008) 102:59–67. doi: 10.1161/CIRCRESAHA.107.159129
38. Miller FJ Jr, Dellsperger KC, Gutterman DD. Pharmacologic activation of the human coronary microcirculation in vitro: endothelium-dependent dilation and differential responses to acetylcholine. *Cardiovasc Res.* (1998) 38:744–50. doi: 10.1016/S0008-6363(98)00035-2
39. Leurgans TM, Bloksgaard M, Brewer JR, Bagatolli LA, Fredgart MH, Rosenstand K, et al. Endothelin-1 shifts the mediator of bradykinin-induced relaxation from NO to H₂O₂ in resistance arteries from patients with cardiovascular disease. *Br J Pharmacol.* (2016) 173:1653–64. doi: 10.1111/bph.13467
40. Hoepfl B, Rodenwaldt B, Pohl U, De Wit C, EDHF. but not NO or prostaglandins, is critical to evoke a conducted dilation upon ACh in hamster arterioles. *Am J Physiol Heart Circ Physiol.* (2002) 283:H996–H1004. doi: 10.1152/ajpheart.01082.2001
41. Kuo L, Chilian WM, Davis MJ. Interaction of pressure- and flow-induced responses in porcine coronary resistance vessels. *Am J Physiol Heart Circ Physiol.* (1991) 261:H1706–H115. doi: 10.1152/ajpheart.1991.261.6.H1706
42. Hein TW, Belardinelli L, Kuo L. Adenosine A_{2A} receptors mediate coronary microvascular dilation to adenosine: role of nitric oxide and ATP-sensitive potassium channels. *J Pharmacol Exp Ther.* (1999) 291:655–64.
43. Hein TW, Kuo L. cAMP-independent dilation of coronary arterioles to adenosine: role of nitric oxide, G proteins, and K_{ATP} channels. *Circ Res.* (1999) 85:634–42. doi: 10.1161/01.RES.85.7.634
44. Hein TW, Wang W, Zoghi B, Muthuchamy M, Kuo L. Functional and molecular characterization of receptor subtypes mediating coronary microvascular dilation to adenosine. *J Mol Cell Cardiol.* (2001) 33:271–82. doi: 10.1006/jmcc.2000.1298
45. Makujina SR, Olanrewaju HA, Mustafa SJ. Evidence against K_{ATP} channel involvement in adenosine receptor-mediated dilation of epicardial vessels. *Am J Physiol Heart Circ Physiol.* (1994) 267:H716–24. doi: 10.1152/ajpheart.1994.267.2.H716
46. Lynch FM, Austin C, Heagerty AM, Izzard AS. Adenosine- and hypoxia-induced dilation of human coronary resistance arteries: evidence against the involvement of K_{ATP} channels. *Br J Pharmacol.* (2006) 147:455–8. doi: 10.1038/sj.bjp.0706622
47. Sato A, Terata K, Miura H, Toyama K, Loberiza FR Jr, Hatoum OA, et al. Mechanism of vasodilation to adenosine in coronary arterioles from patients with heart disease. *Am J Physiol Heart Circ Physiol.* (2005) 288:H1633–40. doi: 10.1152/ajpheart.00575.2004
48. Hedegaard ER, Nielsen BD, Kun A, Hughes AD, Kroigaard C, Mogensen S, et al. K_v7 channels are involved in hypoxia-induced vasodilatation of porcine coronary arteries. *Br J Pharmacol.* (2014) 171:69–82. doi: 10.1111/bph.12424
49. Borysova L, Dora KA, Garland CJ, Burduga T. Smooth muscle gap-junctions allow propagation of intercellular Ca²⁺ waves and vasoconstriction due to Ca²⁺ based action potentials in rat mesenteric resistance arteries. *Cell Calcium.* (2018) 75:21–9. doi: 10.1016/j.ceca.2018.08.001
50. Groves P, Kurz S, Just H, Drexler H. Role of endogenous bradykinin in human coronary vasomotor control. *Circulation.* (1995) 92:3424–30. doi: 10.1161/01.CIR.92.12.3424